Li *et al. Chem Synth* 2024;4:35
DOI: 10.20517/cs.2023.54

Chemical Synthesis

Review

Open Access

Chiral cage materials with tailored functionalities for enantioselective recognition and separation

Tianyu Li[#], Yuan Pan[#], Luyao Ding, Yihong Kang, Xin-Qi Hao, Yujing Guo[*], Linlin Shi[*]

College of Chemistry, Zhengzhou University, Zhengzhou 450001, Henan, China.
[#]Authors contributed equally

[*]**Correspondence to:** Prof. Linlin Shi, Prof. Yujing Guo, College of Chemistry, Zhengzhou University, Zhengzhou 450001, No.100 Science Avenue, Henan, China. E-mail: linlinshi@zzu.edu.cn; yujingguo@zzu.edu.cn

How to cite this article: Li T, Pan Y, Ding L, Kang Y, Hao XQ, Guo Y, Shi L. Chiral cage materials with tailored functionalities for enantioselective recognition and separation. *Chem Synth* 2024;4:35. https://dx.doi.org/10.20517/cs.2023.54

Received: 30 Oct 2023 **First Decision:** 11 Mar 2024 **Revised:** 24 Apr 2024 **Accepted:** 30 May 2024 **Published:** 14 Jun 2024

Academic Editor: Wei Li **Copy Editor:** Dong-Li Li **Production Editor:** Dong-Li Li

Abstract

Chiral chemistry is often regarded as the science of studying the stereostructure and symmetry of organic molecules. It mainly focuses on the presence of chiral centers in specific structures and their impact on conformation, properties, and functions. In this field, researchers explore the special properties and potential applications of chiral compounds through synthesis, separation, and characterization. Here, we aim to provide a detailed overview of diverse functionalized cages based on chiral skeletons and their applications in enantioselective recognition and separation, and a diversity of chiral caged skeletons bearing customized functionalities conducted on the recognition and separation of chiral guests.

Keywords: Chiral cages, separation, self-assembly, synthesis, enantioselectivity

INTRODUCTION

With the continuous development and progress of technology, chiral chemistry has penetrated diverse fields, such as chemistry[1-3], pharmacy[4-6], agriculture[7-9], environmental science[10-12], materials science[13-15], and clinical medicine[16-18]. For example, for the domain of pharmaceuticals, chiral chemistry not only helps us understand the specific biological activity, metabolic pathways, and side effects of drug molecules but also provides a theoretical basis and guidance for designing safer and more effective drug lead compounds[19-23]. In addition to medicine and agriculture, it is widely used in various fields such as materials science, catalyst design, and food additives. For example, functional materials in materials science with

specific photoelectric, mechanical, or conductive properties can be obtained by regulating the spatial arrangement of units in polymer or crystal materials[24-30]. Therefore, chiral chemistry, as an important and complicated discipline, plays an important role in various industries.

Chiral molecular cages are chemical structures with special structures and functions. It comprises chiral molecules with asymmetric spatial arrangement, which gives them unique advantages in optical activity, biological activity, and functionality[31-36]. With the continuous development and progress of synthetic chemistry, new reagents, reactions and synthetic strategies have been continuously applied to fabricate and modify chiral architectures, which has greatly promoted the widespread application of these functional molecules. For example, in biomedicine, the cages with chiral skeletons can serve as drug carriers, stably encapsulating drugs internally and achieving precise release for different diseases by regulating their pore sizes and surface modification[37-41]. In addition, chiral cages can also provide efficient, selective, and reusable reaction environments, thereby promoting organic synthesis reactions with extremely high reactivity (including chemical selectivity, regional selectivity, and stereoselectivity) in catalyst designing and application[42-47]. Furthermore, they are also widely used in fields such as materials science, energy storage and conversion. For example, the battery capacity and cycle life can be highly improved by using some 3D materials in the update and iteration process of battery technology[48-54]. For designing and manufacturing photovoltaic devices, cage-like structures can improve light absorption efficiency and carrier transport speed by adjusting chiral ligands[55-59]. In recent years, significant progress has also been made in preparing nanoscale structures or devices using these functional backbones[60-63]. These practical but powerful structures can be applied to information storage, sensor manufacturing, and micromechanical devices[64]. In summary, chiral molecular cages, as a novel type of material, have shown great potential for application in multiple scientific fields and are constantly developing and innovating, and the chiral molecular cage will undoubtedly bring more surprises and breakthroughs to human society in the future.

Chiral recognition and resolution, as an important technology in various fields, is mainly applied to the separation and identification of chiral molecules[65-78]. Early research on chiral guests mainly focused on physical and chemical methods to determine their chirality. Common methods include optical activity meters, circular dichroism (CD), and optical rotation methods[79-82]. Through chiral recognition, the chirality of molecules can be determined for subsequent resolution, and the separation of chiral molecules is mainly reflected in chromatographic[83-85], crystallization[86], and membrane separation[87-89]. In addition, the chemical synthetic strategies mainly utilize chiral catalysts or sources as key factors to obtain a single enantiomer. In recent years, chiral recognition and resolution technologies have been widely applied in fields such as pharmaceuticals, materials, and food. For example, in the pharmaceutical field, chiral recognition and resolution technology can prepare optically pure drugs, improve drug efficacy, and reduce adverse reactions[90-92], and enantiomers can also be used to prepare materials with optical activity, such as optically active polymers and chiral liquid crystals[93-95]. Not only that, chiral recognition and resolution technology can detect chiral components in food production, such as sugars and amino acids[96,97]. Based on this research background, applying functionalized cages for recognizing and resolution of chiral molecules has also achieved rapid development.

Here, we aim to provide a detailed overview of diverse functionalized cages based on chiral skeletons and their applications in enantioselective recognition and separation (and their limitations) and put forward some guiding principles and guidelines on the relevant mechanisms to promote the development of simply and efficiently generating supramolecular cage materials with high performance, which is also powerful to maintain the continuous and vigorous development of this emerging field. In the context of the rapid development of this field, a review of functionalized cages based on chiral skeletons is necessary and

important to provide meaningful guidance for future research and enable them to achieve better performance in guest recognition and separation with excellent enantioselectivities.

SYNTHESIS AND APPLICATION OF CHIRAL CAGES FORMED WITH CHIRAL BUILDING BLOCKS

In recent years, many examples of constructing chiral cages based on chiral initiation modules have been reported. A significant advantage of this method is that by introducing enantiomeric chiral groups into ligands or metals, the ligand units are endowed with specific chirality, thereby making the assembled molecular cages also chiral. From the perspective of molecular symmetry, this chirality is generally permanent. However, the drawback of this approach is that preparing molecular cages with different configurations requires tedious and complex synthesis steps.

Binaphthalene-derived chiral cages for enantioselective separation

The C_2 symmetric axis of binaphthalene, as an important and intriguing chiral skeleton, widely exists in synthesizing catalysts, natural products, pharmaceutical compounds, and materials. In addition, this axial chirality arising from the restricted rotation around a single bond has recently aroused increasing attention due to its fascinating structure and multidisciplinary applications[98,99]. A pair of chiral covalent organic cages with binol as the backbone and tridiaminoethylamine as the vertices were designed and synthesized by Ramakrishna *et al.*, which was the first example of using binol as the starting material to synthesize chiral imine cages via imine condensation strategy [Figure 1A][100]. The developed structures were further reduced to amine cages so as to increase chemical stability. In addition, the successful synthesis of imine cage was also confirmed by characterization methods such as nuclear magnetic resonance (NMR), mass spectrometry (MS), ultraviolet-visible (UV-Vis) spectroscopy, and single crystal X-ray diffraction analysis, showing that the chiral imine cage contained a C_3 symmetric backbone and possessed a narrow cavity [Figure 1B]. Additionally, the CD experiment result showed a strong Cotton effect, which provided strong backing for the successful synthesis of target cages [Figure 1C]. Meanwhile, chiral cages could effectively recognize the enantiomers of 1,2-cyclohexanediamine (**CA**) owing to different structural changes in the presence of the enantiomeric guests [Figure 1D]. The NMR spectrum indicated that the cage would decompose into different structures after binding to varying guest configurations, which was the reason for the different fluorescence intensities.

Recently, chiral imine cages (**C2**) with [3+6] skeletons were successfully synthesized by Liu *et al.* using the binol derivatives and **CA** enantiomers as the substrates[101] [Figure 2A]. The developed **C2** displayed obvious circularly polarized luminescence (CPL) activity and could selectively recognize chiral substrates based on changes in the CD spectrum. Using **CA** and binol as the most reactive precursors might theoretically lead to forming four types of cages. However, only (***S,R***)-**C2** and (***R,S***)-**C2** were proven to be clearly synthesized through ^{1}H NMR, MS, and single crystal X-ray diffraction analysis. The successful formation of (***S,R***)-**C2** and (***R,S***)-**C2** based on the current protocol was demonstrated by smaller simulated formation energy of -132.4 kcal·mol^{-1}, which were caused by the configuration of (***S,S***)-**DBD** + (***R,R***)-**CA** and (***R,R***)-**DBD** + (***S,S***)-**CA**, respectively. By contrast, the energies of (***R,R***)-**C2** and (***S,S***)-**C2** were -71.5 kcal·mol^{-1}. (***S,R***)-**C2** and (***R,S***)-**C2** were also applied to enantioselective recognition of *rac*-carvone guests. As shown in Figure 2B-G, significant changes in the CD spectra of (***S,R***)-**C2** at 250 nm could be observed obviously with the continuous addition of *D*-carvone. On the contrary, no significant changes were found in the CD spectra after adding *L*-carvone. Similar results were also observed when using (***R,S***)-**C2** as the host molecule. In addition, density functional theory (DFT) calculations were used to explain the mechanism of enantioselective recognition and CH···π interactions between the cage and guest might affect the π-π^* transitions of the binaphthol moieties, leading the intensity change of the CD peak at 250 nm.

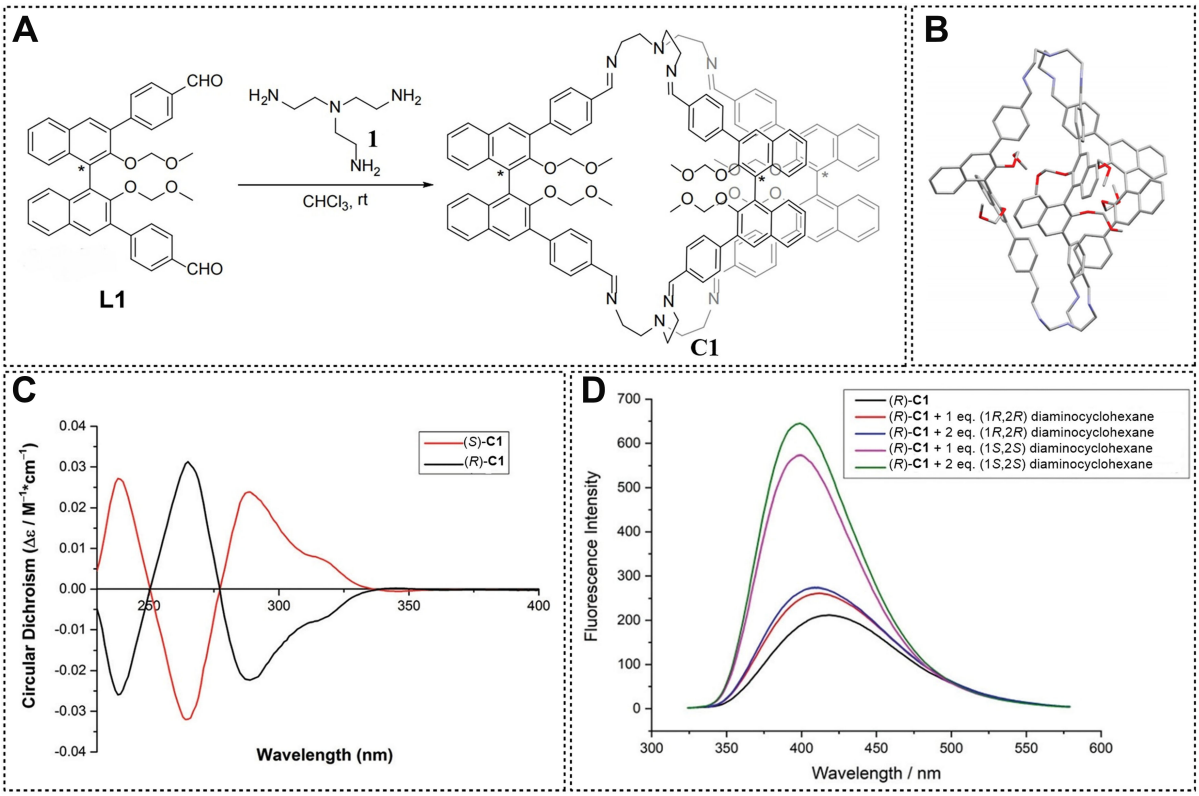

Figure 1. (A) Synthesis of the chiral binol cages via imine condensation. *represents chirality factor; (B) single-crystal structure of **(*R*)-C1**, H atoms and solvents have been omitted for clarity; (C)CD spectra of C1 and (D) fluorescence spectral changes of **(*R*)-C1** upon the addition of (*1R,2R*)-1,2-diaminocyclohexane and (*1S,2S*)-1,2-diaminocyclohexane.

The above two examples both use single configurational ligands to synthesize imine cages, but directly generating supramolecular cages through racemic ligands is even more fascinating. In addition, the characteristics of the imine bond enable it to decompose under harsh conditions such as strong acidity and alkalinity environments. To address this issue, a porous organic cage was successfully designed and synthesized by Cui *et al.* using binaphthylenediamine as the substrate in 2022[102]. This synthesis strategy could effectively avoid the disadvantage of easy hydrolysis during the imine condensation process, and the distinctive structure of 2,4,6-triformylphloroglucinol enabled the keto-enol tautomerism, which caused the transformation of imines into amines during the course of self-assembly following the formation of imine bonds [Figure 3A]. Moreover, the inherent hydrophobicity of the aromatic framework was instrumental in developing encapsulation chemistry, which significantly enhanced the stability of the sample under various challenging conditions. This distinctive property allowed the material to surpass the limits of traditional materials, ensuring it could endure arduous and demanding environments characterized by complex acid-base compositions [Figure 3B]. Significantly, only a cage of homochirality could be obtained using 2,4,6-triformylphloroglucinol and *rac*-Binam as the starting materials, although different cage structures could be theoretically generated. The entropy difference ΔS between the homochirality and heterochirality structures was only 15.11 $J{\cdot}K^{-1}{\cdot}mol^{-1}$ according to the results of DFT calculations. However, the enthalpy difference ΔH was much larger, ranging from 105.35 to 311.94 $kJ{\cdot}mol^{-1}$ [Figure 3C]. The results showed that ΔH favored the formation of a homochiral cage over the heterochiral structures, and the significant energy difference could result in a lower ΔG for the formation of the homochiral cage than that of heterochiral ones, indicating that the cage of homochirality might be a thermodynamically stable conformation. Furthermore, the developed cage could achieve configuration conversion in varying organic solvents [Figure 3A].

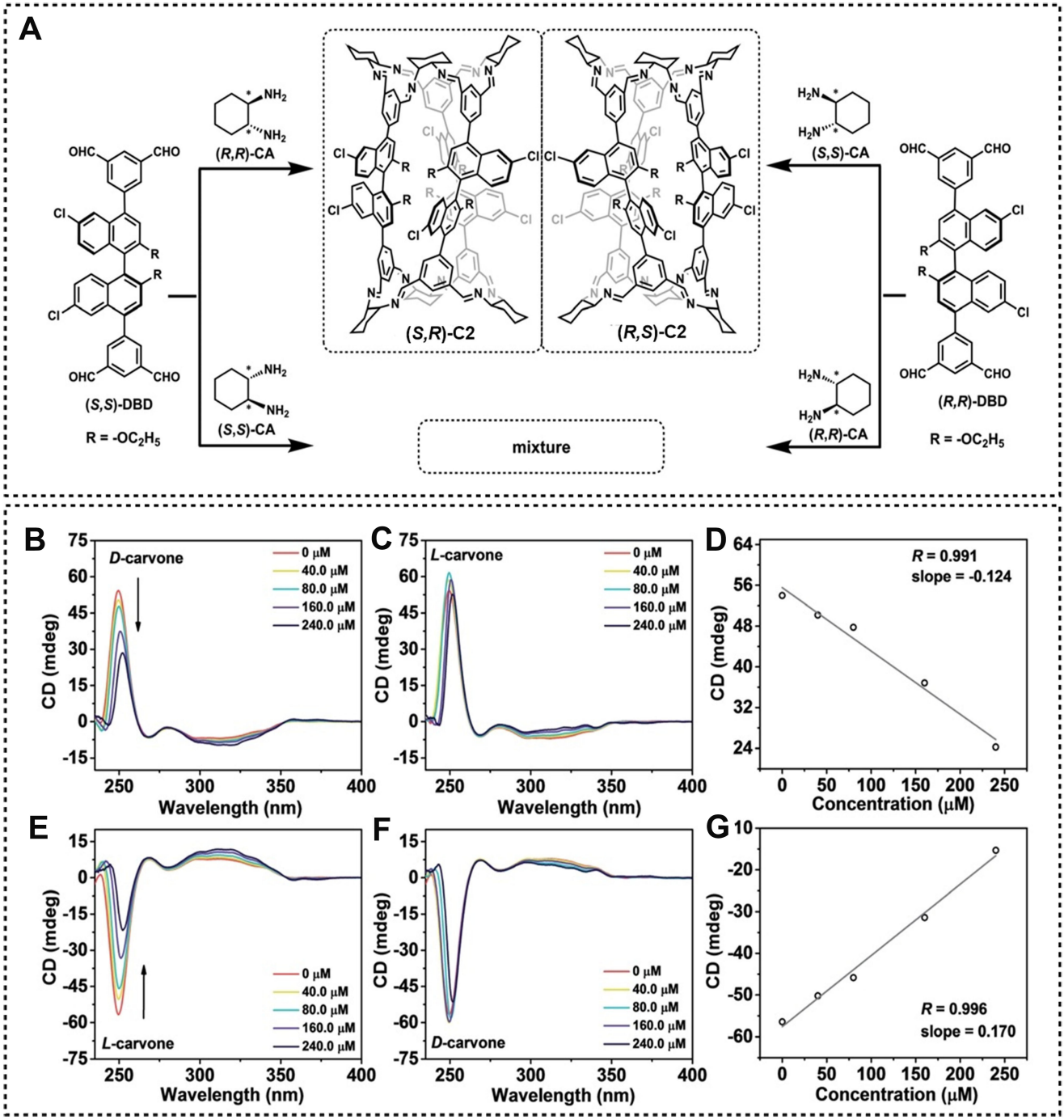

Figure 2. (A) Synthesis of heterochiral porous organic cage **C2**.*represents chirality factor; CD spectra of **(*S*,*R*)-C2** with different concentrations of (B) *D*-carvone and (C) *L*-carvone; (D) The CD intensity at λ = 250 nm *vs.* the *D*-carvone concentration. The CD spectra of **(*R*,*S*)-C2** with various concentrations of (E) *L*-carvone and (F) *D*-carvone; (G) The CD intensity at λ = 250 nm *vs.* the *L*-carvone concentration. CD: Circular dichroism.

Moreover, a series of binol derivatives were chosen as the guests for enantioselective recognition, and different intensity changes of fluorescence could be obviously observed due to distinct configurations of binaphthol derivatives, indicating the unique recognition ability for various axially chiral aromatic racemates based on the enantiopure **C3** [Figure 3D].

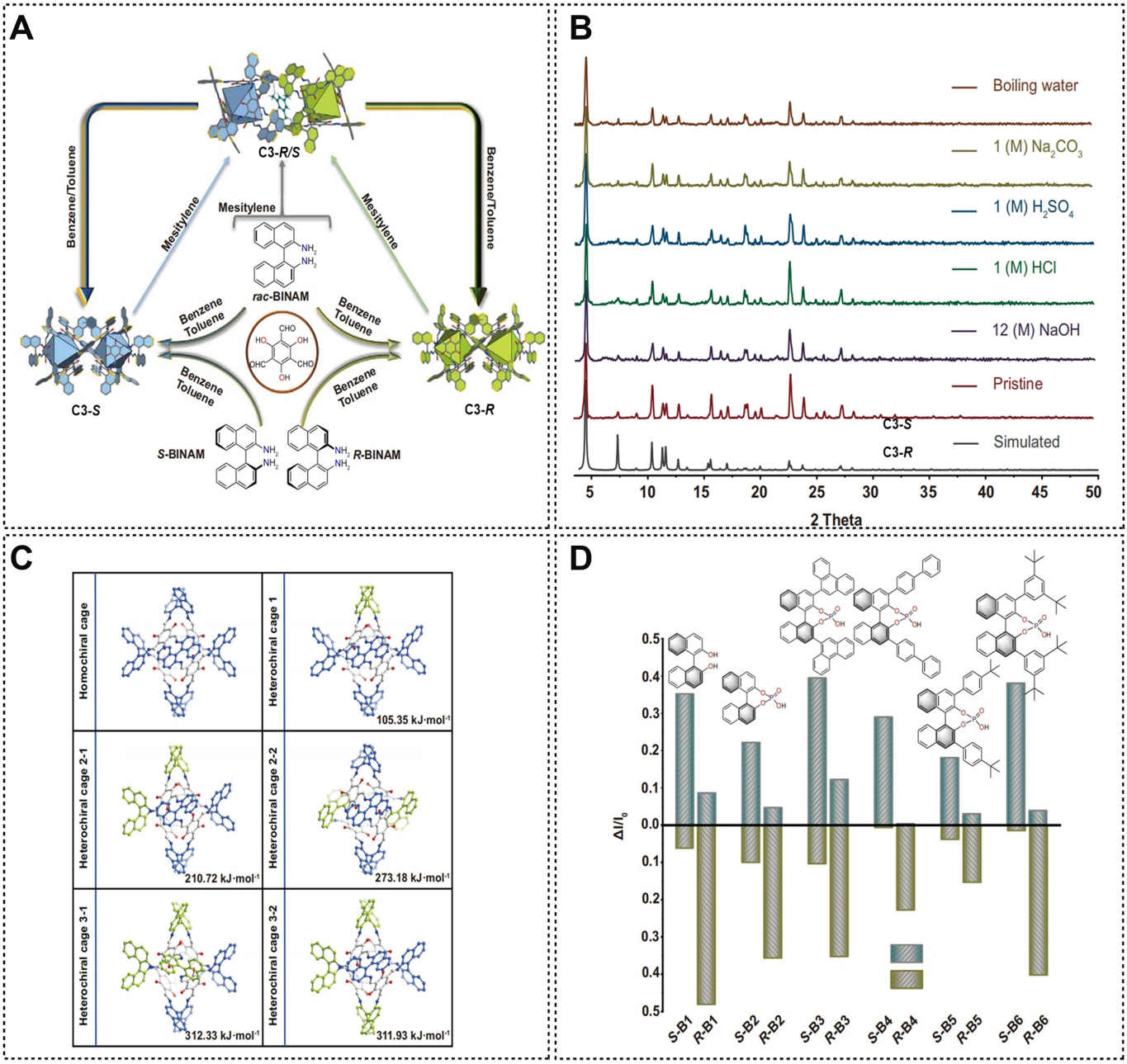

Figure 3. (A) The synthesis of cage and the reversible supramolecular structural transformation between homochiral and racemic structures under different solvents; (B) PXRD patterns of **C3-S** under different harsh conditions; (C) the optimized cage structures based on DFT calculations and (D) ratio of luminescent intensity. PXRD: Powder X-ray diffraction; DFT: density functional theory.

Helicene-derived chiral cages for enantioselective separation

Helicene, as a non-planar helical structure composed of positively fused aromatic rings (total number ≥ 4), exhibits remarkable cross properties due to its unique helical π conjugation system. The geometric shape and unique optical properties of the helix structures make them the promising candidate materials for circularly polarized light devices, asymmetric catalysis, chip switches, chiral recognition, and other fields[103,104]. In 2018, Malik *et al.* developed the synthesis of covalent organic cages using chiral building

blocks derived from ditopic aldehyde-substituted helicene[105], which was the first example of chiral imine cages synthesized by imine condensation of helicene. As shown in Figure 4A, precursors ***M*-L2** and ***P*-L2** were obtained through Sonogashira coupling of helix alkyne with iodobenzaldehyde. Subsequently, a supramolecular cage with helicene structure was generated through the conventional condensation process of amino and aldehyde groups in 67% to 69% yield, and the corresponding [3+2] structure was determined by ^{1}H NMR and MS. The author discovered that this cage exhibited a structurally chiral conformation by further examining the crystal structure [Figure 4B]. The conformation involved three lateral arms that twisted into a triple helix. In ***M,M,M*-C4**, the helicene units were arranged in a propeller-like manner, with the ends pointing inward towards the cavity of the molecule, which created an open cave that could be accessible from three directions. The three lateral arms rotated clockwise around a pseudo-C_3 axis, resulting in a left-handed triple helix. What is more, ***P,P,P*-C4** displayed a right-handed triple helix due to the inherent chirality of helicene. This unique chiral triple helix backbone caused selective recognition and separation of chiral molecules, such as some aromatic racemic compounds. As shown in Figure 4C, chiral cages exhibited excellent enantioselective encapsulation ability for 1-phenylethylamine and 1-phenylethanol (PE). However, the enantiomeric excess (*ee*) values of binol were very low, possibly due to the large steric hindrance of the guests affecting the resolution ability of cages. At the same time, the enantioselectivity of chiral **L2** to 1-phenylethylamine showed very low *ee* values, indicating that the enantioselectivity originated from the integral structure of the cage rather than the discrete helicene moieties.

In 2019, a series of self-assembled supramolecular cages were designed and synthesized by Schulte *et al.* using helix-palladium complex as the chiral source[106] [Figure 5A]. The pyridyl ligand could selectively combine with Pd(II) cations to form an achiral *meso*-cage **C5*meso***. Meanwhile, homochiral cage **C5*P/M*** was formed using enantiopure **L3**, while cage **C6*P/M*** with a larger cavity inside was formed using a longer **L3** derivative, which could bind with optical isomers of chiral guests in different degrees. The chiroptical properties of these cages allowed them to encapsulate and identify the achiral guests with varying lengths, as the guests could either compress or elongate the cavity by changing the helical pitch of the helicenes. In addition, the dimer of **C6*P/M*** had also been successfully synthesized and the CD spectra of the enantiomers of **C6*P/M*** and **L4*P/M*** gave perfect mirror images, respectively [Figure 5B]. More importantly, this type of cage could not only wrap negatively charged guests through electrostatic interactions but also effectively fix them inside, showing its potential to recognize guests. **C6*P*** and **C6*M*** were respectively employed to recognize camphor sulfonate, in an attempt to explore the application of chiral cages in recognizing chiral guests. Characteristic downfield shifts were observed for the H^a proton resonance [Figure 5C]. It was fascinating to note that both enantiomers of the guest showed different binding behaviors when they were exposed to the same chiral cage. The combination **12*S*@C6*P*** exhibited the same behavior as the enantiomeric system **12*R*@C6*M***, with a binding constant of approximately 560 M^{-1}. In contrast, the diastereomeric combinations **12*R*@C6*P*** and **12*S*@C6*M*** displayed a greater extent of NMR signal shifts and a binding constant of approximately 1,010 M^{-1}. Nevertheless, no significant differences were observed in the analysis of chiral guest identification between **C5*P*** and (*1R*)-and (*1S*)-camphor sulfonate anions owing to the restricted capacity of the cavity, which was a crucial factor in the binding of guests. Furthermore, these helicene backbones could be utilized to effectively identify achiral anionic guests with different sizes [Figure 5D].

Other skeletons-derived ciral cages for enantioselective separation

In 2020, Lei *et al.* developed the fabrication of chiral imine cages by introducing the **CA** enantiomers as chiral elements into the corresponding structures[107]. The synthesized cages were proved to possess the unique stability in water, and the water solubility of the cage came from the triscationic nature of the important precursor **L5** [Figure 6A]. A fantastic mirror symmetry relationship was detected between *S*-**C7**$^{3+}$·3Br$^-$ and *R*-**C7**$^{3+}$·3Br$^-$ through the CD spectra analysis, and the CD signal of the cage disappeared

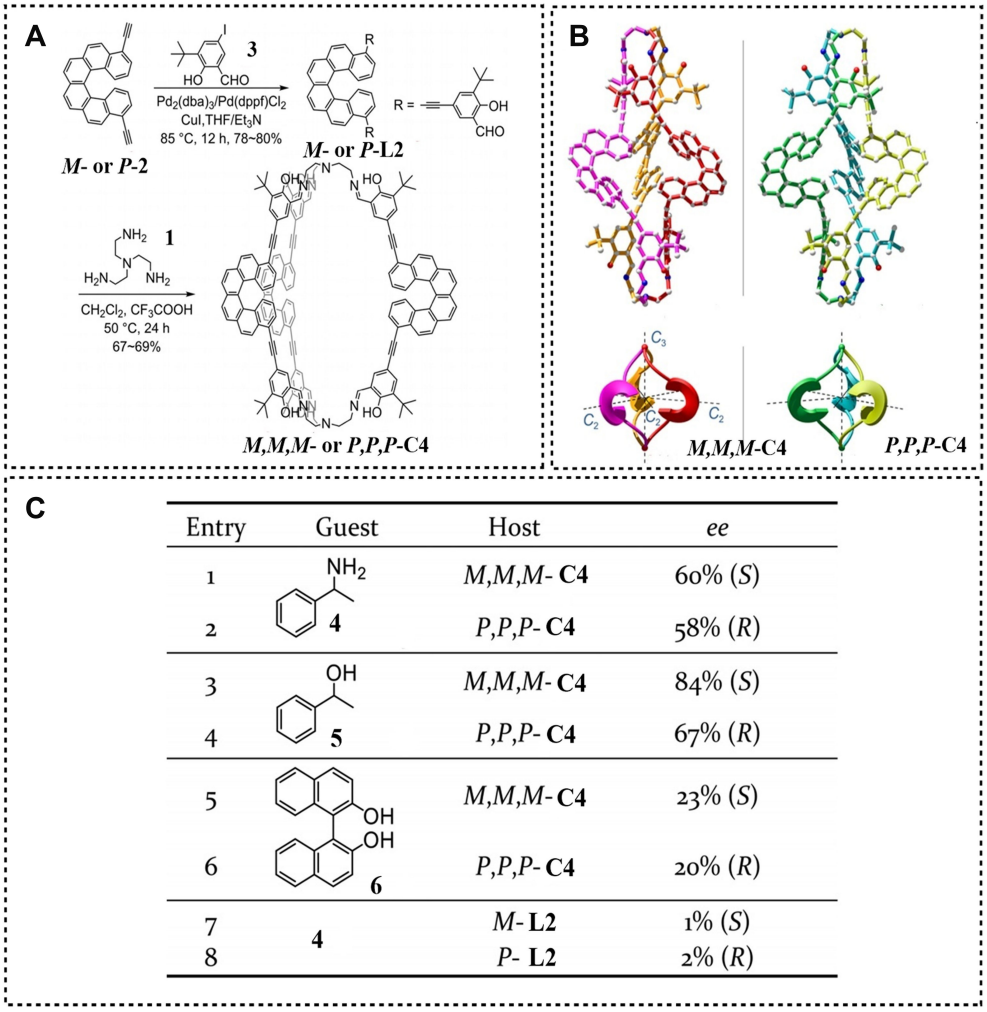

Figure 4. (A) Synthetic route to organic cages by using helicene derivatives as building blocks; (B) crystal structures of organic cages ***M,M,M*-C4** and ***P,P,P*-C4** and schematic representations of ***M,M,M*-C4** and ***P,P,P*-C4** illustrating the D_3 symmetry and the triple-stranded helical structure and (C) data of chiral adsorption experiments.

when the enantiopure **CA** was replaced by racemic **CA**, indicating that narcissistic self-sorting occurred [Figure 6B]. The chiral cavity of the cage was believed to correspond to the separation of chiral molecules through hydrophobic effects. For example, 1,2-epoxybutane could be enantioselectivly separated by cages [Figure 6C]. The ^{1}H NMR spectra [Figure 6C] showed that the resonances of (*R*)-1,2-epoxybutane experienced significant upfield shifts with the addition of cage *S*-**C7**$^{3+}$·3NO_3^-. ^{1}H NMR titration experiments revealed that the *Ka* value of (*R*)-1,2-epoxybutane was approximately 35 M^{-1}, whereas the *Ka* value of (*S*)-1,2-epoxybutane was too small to be accurately determined. On the other hand, some appropriately sized linear molecules could be encapsulated in cages due to hydrophobic effects, such as ethane, 1-chloropentane, 1-bromopentane, *etc.* [Figure 6D]. The root of cage encapsulation ability lay in hydrophobic effects and electrostatic interactions. The aforementioned interplay was responsible for the selective trapping and encapsulation processes, enabling the dynamic management of materials with complex structures.

In 2023, two types of enantiopure tetrahedral metal cages were prepared by Li *et al.*, which were assembled from triazatruxene-based subcomponent **L6**, iron (II) bis (trifluoromethanesulfonyl) imide (triflimide,

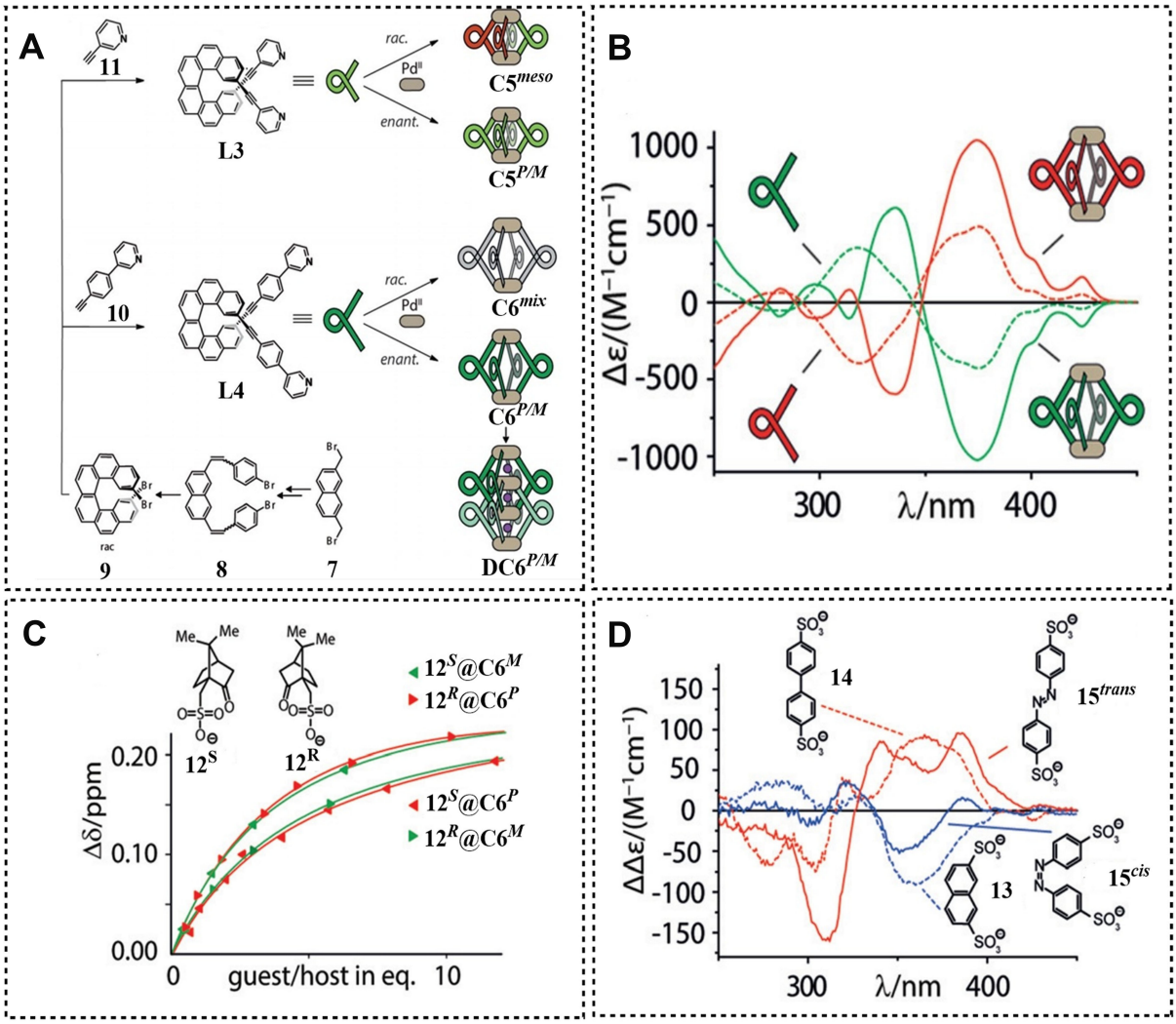

Figure 5. (A) Synthesis of cages; (B) CD spectra of ligands **L4*P/M*** and cages **C5*P/M***; (C) comparison of the binding isotherms and difference; (D) CD spectra of **13@C6*P*** and **14@C6*P*** as well as **15*trans*@C6*P*** and **15*cis*@C6*P***. CD: Circular dichroism.

Tf_2N^-), and the chiral monoamine[108]. The synthesized cage compounds had been shown to effectively induce single chirality at the position of metal vertices due to spatial effects. As expected, the CD signals of ***Δ/Λ*-C8** and ***Δ/Λ*-C9** demonstrated the formation of enantiomers [Figure 7A]. In addition, the developed cage could serve as the host to recognize a series of complex steroid guests. As shown in Figure 7B, a significant change of proton signal in the ^{1}H NMR spectrum was observed with the addition of spironolactone (SP) or epimer of SP (ESP), and the aromatic region signal of the cage broadened after the addition of SP due to the tight binding between the cage and the guest, indicating the desymmetrization of the cage framework after encapsulation of the guest on the timescale of NMR chemical shifts [Figure 7C]. Meanwhile, although ESP⊂ Δ/Λ-**C8** both exhibited sharp proton signals, the corresponding signals were significantly different, which proved that ESP⊂***Δ*-C8** and ESP⊂***Λ*-C8** were diastereomers. Some non-covalent interactions based on CH-π interactions and CH···O hydrogen bonds could be observed clearly owing to high binding affinity [Figure 7D]. This three-dimensional network of non-covalent interactions within the host cavity endowed the cage with the ability for the enantioselective recognition and separation application. The values obtained for the binding constants of the complexations between SP and ***Δ*-C8** as well as ***Λ*-C8** were found to be

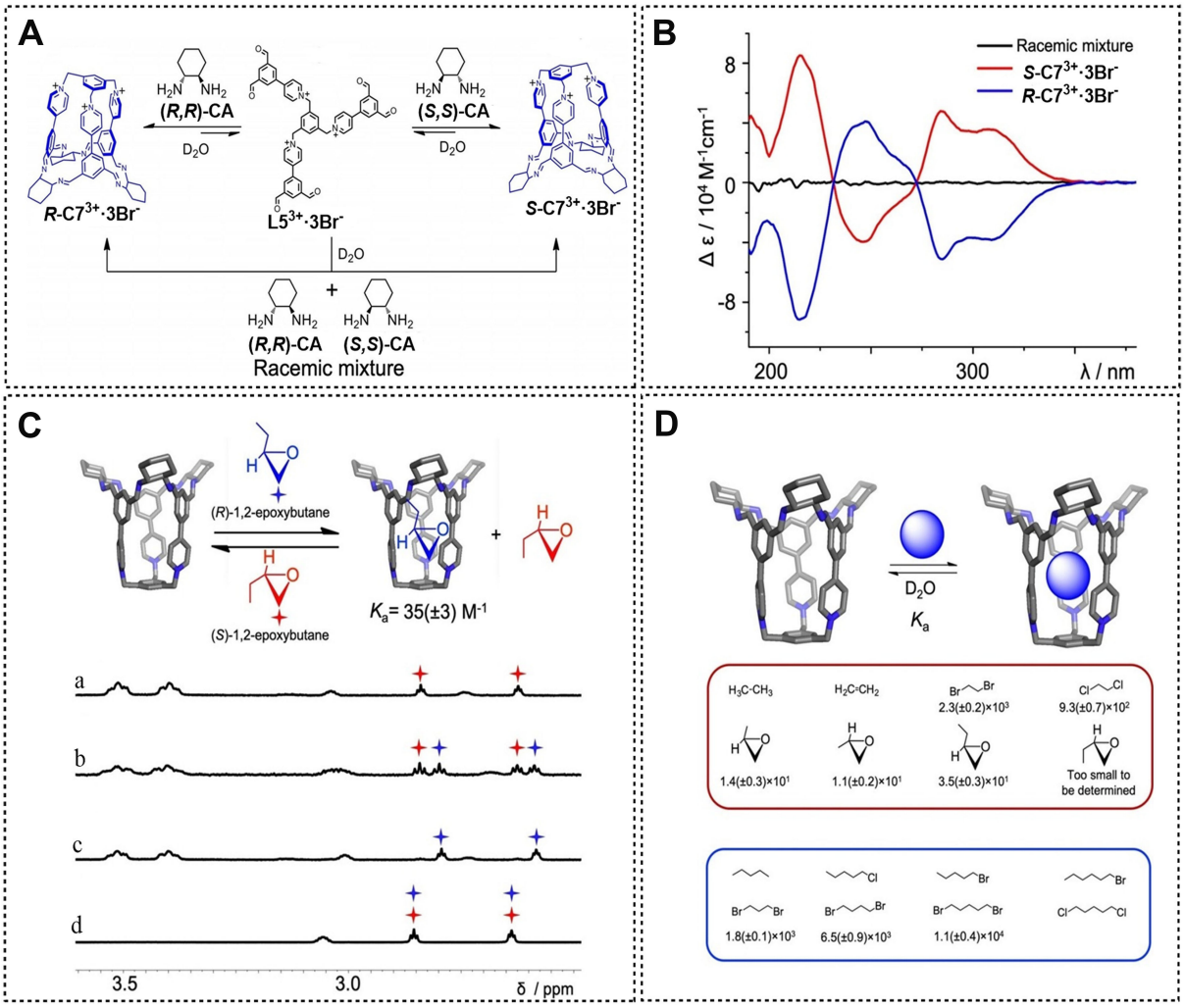

Figure 6. (A) Synthesis of *S*-**C7**$^{3+}$·3Br$^-$ and *R*-**C7**$^{3+}$·3Br$^-$; (B) CD spectra of *S*-**C7**$^{3+}$·3Br$^-$, *R*-**C7**$^{3+}$·3Br$^-$, and the unseparated racemic mixture; (C) partial ^{1}H NMR spectra of a mixture of *S*-**C7**$^{3+}$·3NO_3^-, host-guest complexes and *rac*-1,2-epoxybutane; and (D) host-guest chemistry of *S*-**C7**$^{3+}$ in D_2O. CD: Circular dichroism; NMR: nuclear magnetic resonance.

5.58 × 10^6 and 3.48 × 10^5 M^{-1}, respectively. On the other hand, the binding constants of ***Λ***-**C8** and ***Λ***-**C8** for ESP were determined to be 1.34 × 10^6 and 3.45 × 10^7 M^{-1}, respectively, suggesting that the cage could effectively recognize the enantiomers of ESP and SP. Furthermore, the interaction between canrenone and ***Λ***-**C8** formed a 1:2 complex. Other steroids were also selected for enantioselective recognition exploration, and the enantiomer cages bore different recognition abilities for the guests [Figure 7B].

In 2018, Hou *et al.* reported the formation of octahedral chiral supramolecular cages to effectively separate binol enantiomers[109]. The tridentate ligand based on 2-(pyridin-3-yl)-1H-imidazolo could be generated via an effective coordination between $Fe(BF_4)_2{\cdot}6H_2O$ with imidazolo ligand [Figure 8A]. Subsequently, the target chiral cage structures were successfully produced via the coordination-driven self-assembly process in dimethyl sulfoxide (DMSO) solution. Su introduced enantiopure *R*- or *S*-binol into a solution of ***rac*-C10** to initiate the gradual formation of co-crystals through the vapor diffusion of diethyl ether. As a result, the single crystals of ***S*-binol@*Λ*-C10** and ***R*-binol@*Λ*-C10** enantiomers were successfully obtained, respectively. On the other hand, the enantiomer of binol could also be added during the transformation from ligand to

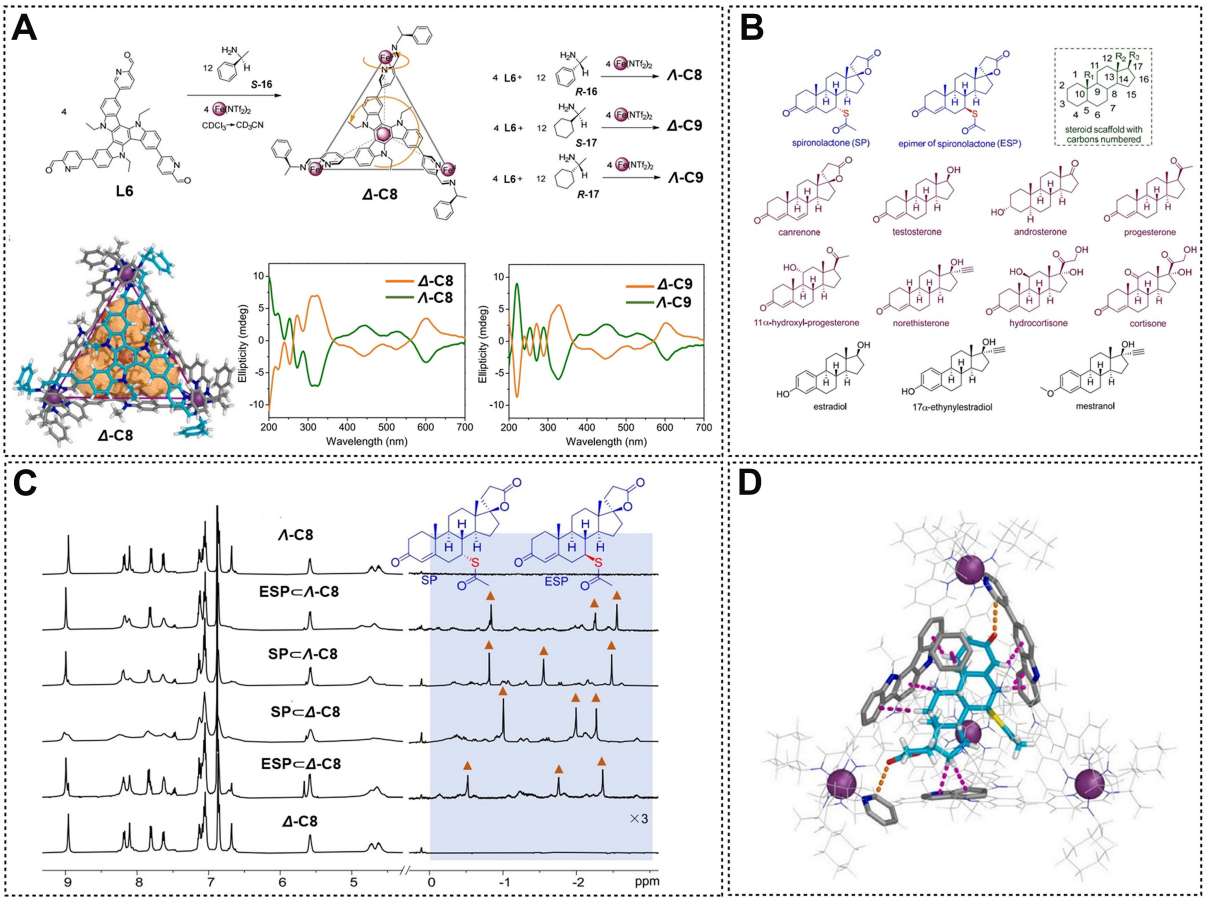

Figure 7. (A) Self-assembly of enantiopure cages **C8** and **C9,** crystal structures of Δ**-C8** and CD spectra of cages; (B) steroid guests investigated for binding with Δ**-C8** and Λ**-C8**; (C) host-guest complexations of the enantiomers of **C8** with SP and ESP; and (D) crystal structure of SP⊂Δ**-C8**. CD: Circular dichroism; SP: spironolactone; ESP: epimer of spironolactone.

product through *in situ* self-assembly process, and the configurations of ***Δ*-C10** and ***Λ*-C10** were confirmed by various methods such as NMR, MS and CD analysis. More importantly, the separation techniques demonstrated that chiral cages could recognize and separate enantiomers of binol [Figure 8B and C]. Three axial chiral compounds were tested in order to explore the enantioselective separation ability of chiral cages. As expected, the cage demonstrated good separation ability with high *ee* values. The ability of **C10** to separate enantiomers came from hydrophobic interactions. Guests in water were captured by **C10**, and the binding rates between different configurations of guests and **C10** varied, which was the key for **C10** to separate enantiomers. Interestingly, the cages could be recycled and reused multiple times due to their good stability. Furthermore, these homochiral cages might have potential applications in asymmetric photocatalysis and photoelectronic devices due to the visible region metal-ligand charge transfer (MLCT) absorption and redox properties of Fe^{3+}/Fe^{2+}.

In 2021, an unprecedented lanthanide chiral metal cage with a "cage in cage" structure was reported by Zhu *et al.*[110]. $\mathbf{H_3L8}$ with C_3 symmetry was deliberately designed and synthesized from *L*-phenylalanine and 1,3,5-benzenetricarboxylic acid through four-step transformations to achieve a satisfactory overall yield. The homochiral cage was obtained by reacting $\mathbf{H_3L8}$ and $LaCl_3$ in a hot solution for two days. This resulted in a "dual-walled" structure with an octahedral internal hollow cavity [Figure 9A]. Four L8 ligands, arranged in a "stretch" configuration, were coordinated with La^{3+} to synthesize the internal cage. Meanwhile, another set

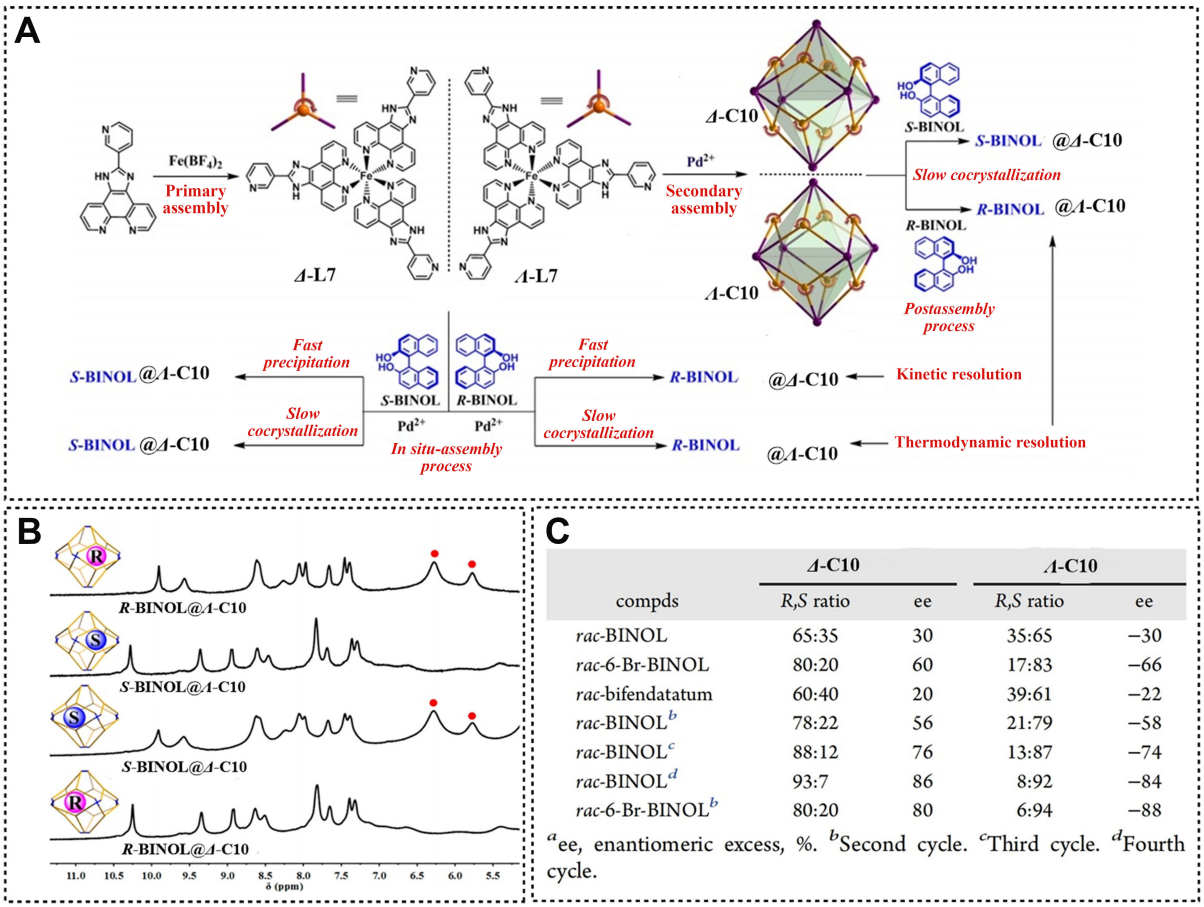

compds	Δ-C10		Λ-C10	
	R,*S* ratio	ee	*R*,*S* ratio	ee
rac-BINOL	65:35	30	35:65	−30
rac-6-Br-BINOL	80:20	60	17:83	−66
rac-bifendatatum	60:40	20	39:61	−22
rac-BINOL[b]	78:22	56	21:79	−58
rac-BINOL[c]	88:12	76	13:87	−74
rac-BINOL[d]	93:7	86	8:92	−84
rac-6-Br-BINOL[b]	80:20	80	6:94	−88

[a]ee, enantiomeric excess, %. [b]Second cycle. [c]Third cycle. [d]Fourth cycle.

Figure 8. (A) Synthetic route for ***rac*-C10**; (B) ^{1}H NMR enantiodifferentiation experiments for capture of *R*/*S*-binols by **Δ/Λ-C10**. Red circles denote signals of encapsulated guests; and (C) enantioselective separation results. NMR: Nuclear magnetic resonance.

of four L8 ligands, arranged in a "fold" configuration, were coordinated with the same metallic compound to construct an external cage enclosing the internal one, forming an octahedral cage. Importantly, the ligands, which had a "stretch" or "fold" arrangement, formed a close stack through powerful intermolecular π-π stacking and hydrogen bonding interactions. The complex "cage in cage" structure, which had multiple chiral microenvironments, laid the foundation for its ability to achieve enantioselective separation. Racemic PE, racemic 2,3-dihydroquinazolinones (DHQZs) and their derivatives were selected for the enantioselective recognition and separation. Satisfactory *ee* values could be obtained through the enantioselective recognition and separation process using the synthesized cages as the hosts [Figure 9B]. The authors also conducted additional investigations into the molecular structure to elucidate the mechanism of enantioselective separation. The cage cavity contained 24 hydrophilic amide groups and the gaps between the cages could serve as locations for enantiomer separation, which gave the cage the ability to recognize and separate enantiomers. The *S*-enantiomer was captured more effectively by the cage, successfully separating the enantiomer due to differences in binding energies. Therefore, this cage molecule provided a promising platform for the resolution of chiral drugs, demonstrating excellent separation and reusable capabilities.

SYNTHESIS AND APPLICATION OF GUESTS INDUCED ENANTIOPURE CAGES

Metal-organic cages synthesized through the self-assembly of achiral ligands and achiral metals generally

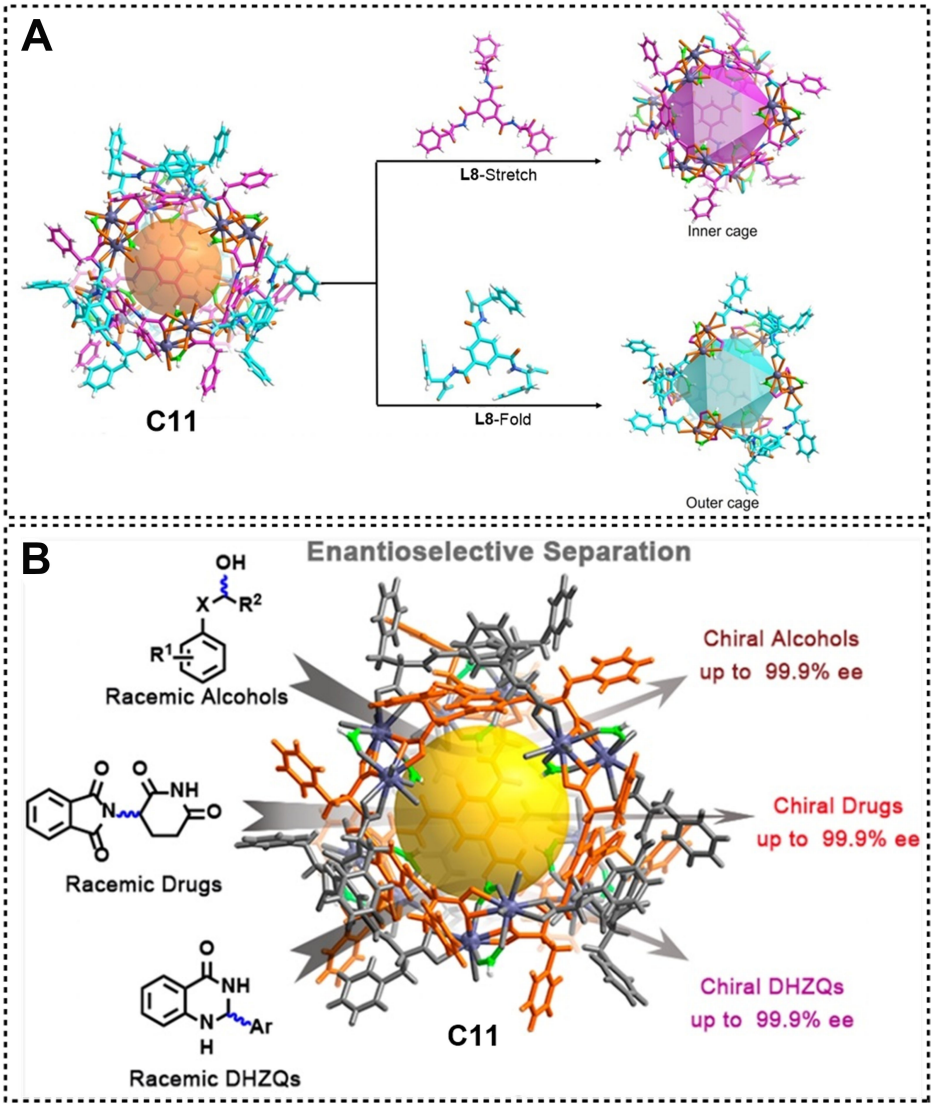

Figure 9. (A) View of the structures of the dual-walled coordination cage and its octahedral inner (purple) and outer (cyan) cage assembled by the flexible ligand and lanthanum ion; and (B) schematic diagram of enantiomer separation results.

exist in the form of racemic mixtures in solution and solid phase, as all metal centers can generate chiral configurations and give the cage structure a certain degree of chirality. Importantly, it is necessary to separate the racemes into enantiopure metal-organic cages aiming to equip these cages with more meaningful applications. Introducing chiral guest-induced cages to generate specific chirality in the reaction system is effective, which has the advantage of avoiding the complex steps in synthesizing chiral ligands. However, choosing the appropriate guests is a challenge because the guests not only need to have strong binding ability with cages but also have a suitable stereo structure to affect the twisting of ligand units on cages, which can make cages chiral.

In 2019, a chiral tetrahedral cage was successfully generated by Zhang *et al.* via coordination-driven self-assembly[111], as the L9 could be positioned on each face in a clockwise or counterclockwise direction and the octahedral vertices of the tetrahedron could be *Δ* or *Λ* partial chirality. Racemic cryptophane (*rac*-CRY) was added to the solution of **C12** to form a "cage in cage" complex [Figure 10A]. Interestingly, the ^{1}H NMR

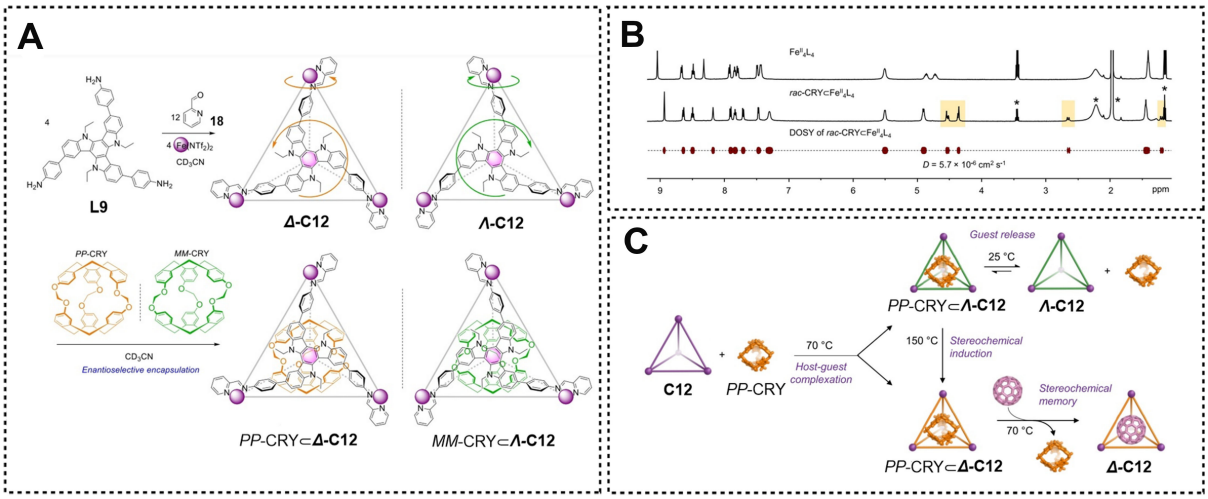

Figure 10. (A) Subcomponent self-assembly of **C12** and enantioselective encapsulation of *rac*-CRY by **C12**; (B) ^{1}H NMR spectra of **C12** and CRY⊂**C12**, and DOSY spectrum of CRY⊂**C12**. The peaks of the encapsulated CRY have been highlighted with a light orange background. *indicates Solvent peaks from diethyl ether, water, and acetonitrile; and (C) stereochemical information transfer from CRY to **C12**. *rac*-CRY: Racemic cryptophane; NMR: nuclear magnetic resonance; DOSY: Diffusion Ordered Spectroscopy.

signal of the complex only showed one set of peaks, indicating a pair of enantiomers in solution [Figure 10B]. In addition, the structures of the enantiomeric complexes had been proved through single-crystal X-ray diffraction, Nuclear Overhauser Effect Spectroscopy (NOESY), and Correlation Spectroscopy (COSY) analysis, which suggested that the cage could selectively recognize and encapsulate CRY in a three-dimensional space. The configuration of *PP*-CRY⊂**Λ-C12** could change into that of *PP*-CRY⊂**Δ-C12** with the temperature increase, and the corresponding configuration could be maintained for one month [Figure 10C]. The transformation of these configurations was attributed to the different binding abilities of the host and guest (the binding constant of *PP*-CRY⊂**Δ-C12** was 530 times that of *PP*-CRY⊂**Λ-C12**), which could be attributed to the differences in three-dimensional configurations affecting the π-π interaction between the host and guest. In addition, the complex could further encapsulate Cs^{+} ion and xenon atom and could potentially be beneficial for applications that relied on molecular recognition, such as catalysis, separations, drug delivery, and sensing.

Recently, Xue *et al.* reported the designation and formation of a triangular chiral cage using Fe^{2+} and an electron-deficient ligand via self-assembly. When the pyridine triazole moieties of the ligand coordinated with the metal vertexes, the ligand would twist in a clockwise or counterclockwise direction, giving rise to the enantiomer cages[112] [Figure 11A]. A diastereomeric cage **C14** was synthesized when the H atom on the pyridine group was replaced by the chiral molecule, and this structure could be verified by two sets of peaks in the 1H NMR spectrum. The diastereomeric ratio (d.r.) value came from the fact that when ligands with chiral groups bound to Fe ions in the synthesized cage, the chiral environment affected the spatial arrangement of the cage vertices, resulting in two cages with different energies. Meanwhile, this value could be controlled by fullerenes and their derivatives as guests due to the different binding abilities of the two hosts. More importantly, **C14** diastereomers both had flat ligand cores and enclosed cavities, thus rendering **C14** a good prospective host for large π-extended guests. Meanwhile, diastereomers of **C14** had distinct binding abilities towards guests due to the difference in rigid three-dimensional structures. The *d.r.* value changed when *MM*-CRY-A was added to the solution of a cage [Figure 11B], indicating that the cage could improve its host-guest binding ability by changing its three-dimensional structure. These results indicated that the cage possessed the superior performance of enantioselective recognition and separation to CRY

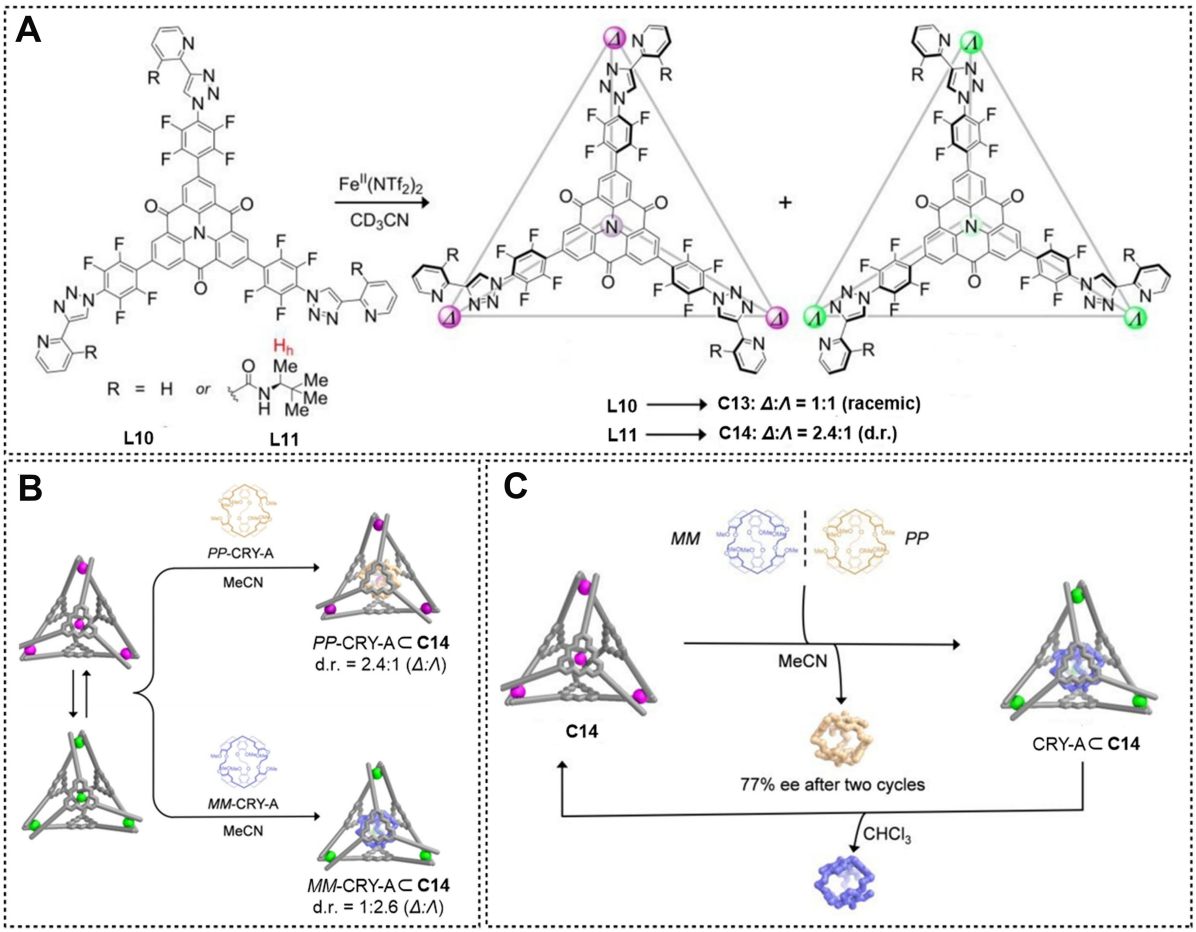

Figure 11. (A) Self-assembly of cages **C13** and **C14** from ligands **L10** and **L11**, respectively; (B) schematic showing the stereochemical communication between **C14** and CRY-A; and (C) schematic showing the enantioselective resolution of CRY-A by cage **C14** in acetonitrile and the recycling of **C14** in chloroform.

enantiomers. Two equivalents of racemic CRY-A were added to an acetonitrile solution of **C14** to test the separation ability of cage **C14** and the reaction mixture was maintained at 343 K for 30 min. The host-guest complex CRY-A⊂**C14** was isolated by precipitation with diethyl ether and evaporation of the excess diethyl ether, and the *ee* value could increase to 77% after two cycles [Figure 11C]. Notably, the cage had good selective encapsulation ability for fullerene and its derivatives due to the varying solubility of the guests in an organic solvent.

Inspired by these achievements, a chiral lanthanide metal tetrahedral cage was successfully synthesized by introducing guests into the solution by Hu *et al.*[113]. The sandwich Eu_3L_3 type complexes could not form due to the introduction of the guest disrupting the π-π interactions between ligands [Figure 12A]. Interestingly, the enantiopure Λ-$Eu_4(L^{C1})_4$ cage was successfully synthesized in the presence of excessive amounts of *S*-binol or *R*-spriol [Figure 12B]. The ability of the cage to capture guests came from the π-π interactions between the host and guest, which was influenced by the differences in three-dimensional structure. The binding constant between the cage and the guests further supported this hypothesis. For example, the apparent binding constants of Λ-$Eu_4(L^{C1})_4$ toward *R*-spriol and *S*-spriol were determined to be 1.74×10^5 M^{-1} and 197 M^{-1}, respectively, indicating that the tetrahedron cage could effectively recognize enantiomers of spriol. In addition, Λ-$Eu_4(L^{C1})_4$ and Δ-$Eu_4(L^{C1})_4$ exhibited excellent CPL signals (dissymmetry factor g_{lum} up to

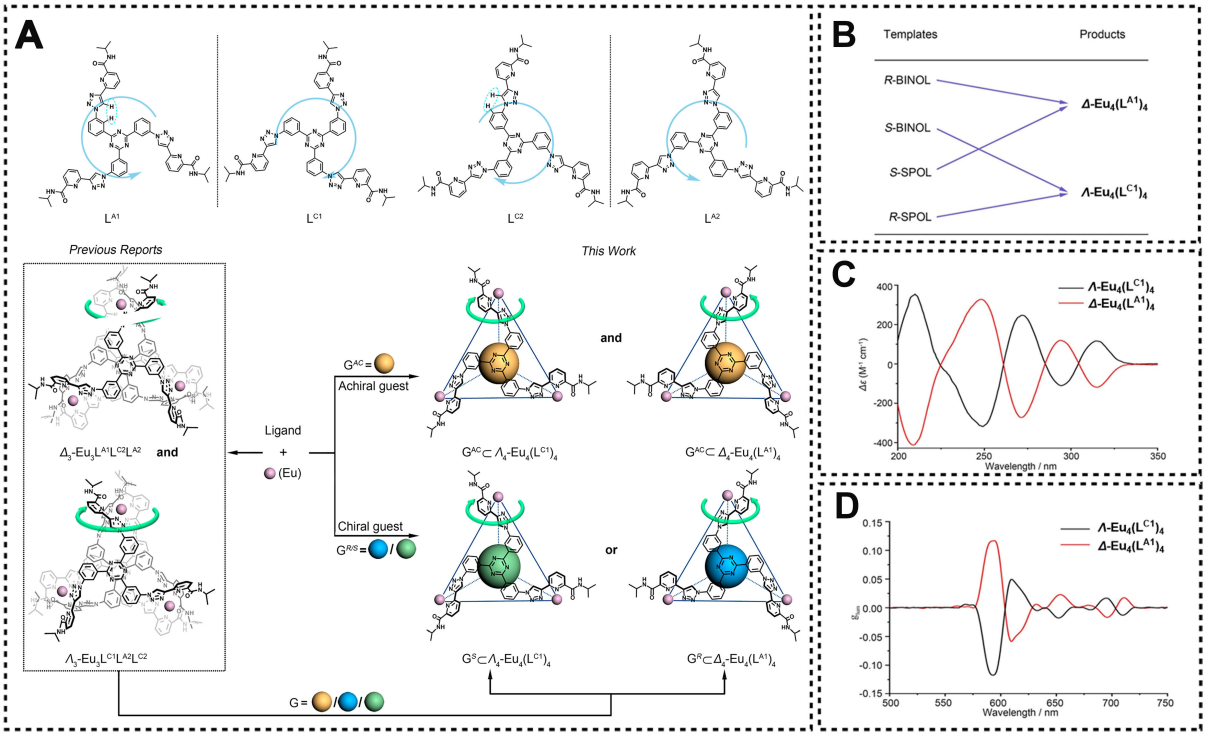

Figure 12. (A) Definition of four modes of ligand (**L12**) and guest-driven self-assembly/transformation showing chiral induction of Eu_4L_4 tetrahedral cages; (B) chiral induction relationship between templates and the tetrahedral cage; (C) CD spectra of Λ-$Eu_4(L^{C1})_4$ and Δ-$Eu_4(L^{A1})_4$; and (D) circular polarized luminescence spectra of Λ-$Eu_4(L^{C1})_4$ and Δ-$Eu_4(L^{A1})_4$. CD: Circular dichroism.

±0.125) [Figure 12C and D], which proved the potential applications in fields such as asymmetric catalysis and biological activity.

In 2021, a water-soluble anionic homochiral octahedral cage was developed by Wu *et al.* using four triacylhydrazone ligands and six Ga^{3+} cations as substrates through coordination-driven self-assembly [Figure 13A][114]. The homochirality of the cage came from the coordination of Ga^{3+} in $\mathbf{C15}^{18-}$ with the ligand, resulting in two enantiomeric configurations. The cage was proved to have good water solubility due to its 12 sulfonic acid units and could remain in water for a month without decomposition. Additionally, the interior of the cage formed a triangular macrocycle that served as a potential external binding site and contained four windows, each encircled by the standing residues as "pillars". The current cage material was selected for the application of enantioselective recognition based on its unique structure, and a large range of guests were systematically explored for the encapsulation, demonstrating the excellent performance of the cage due to hydrophobic effect and coulombic interactions. As shown in Figure 13B and C, the molecular size of the blue compounds was close to the inner cavity size of the cage, so the rate of host guest exchange might be slower at room temperature on the ^{1}H NMR timescale. Relatively speaking, green molecules had a smaller size and could smoothly enter the cavity of the cage for host-guest recognition and encapsulation. In addition, red compounds could effectively bind to the periphery of the cage and undergo rapid host guest exchange on the ^{1}H NMR timescale at room temperature due to their large volume and certain water solubility. More importantly, the racemic cages could transform into enantiopure cages with the addition of chiral guests. As shown in Figure 13C, the ^{1}H NMR signals of cage M_6-$\mathbf{C15}^{18-}$ were significantly weakened with the addition of *L*-**43**, indicating the formation of a thermodynamiclly more stable P_6-$\mathbf{C15}^{18-}$ complex [Figure 13D]. Through hydrophobic effects and multiple binding sites, **C15** could bind to guest molecules internally or externally. One of **C15** enantiomers became thermodynamically

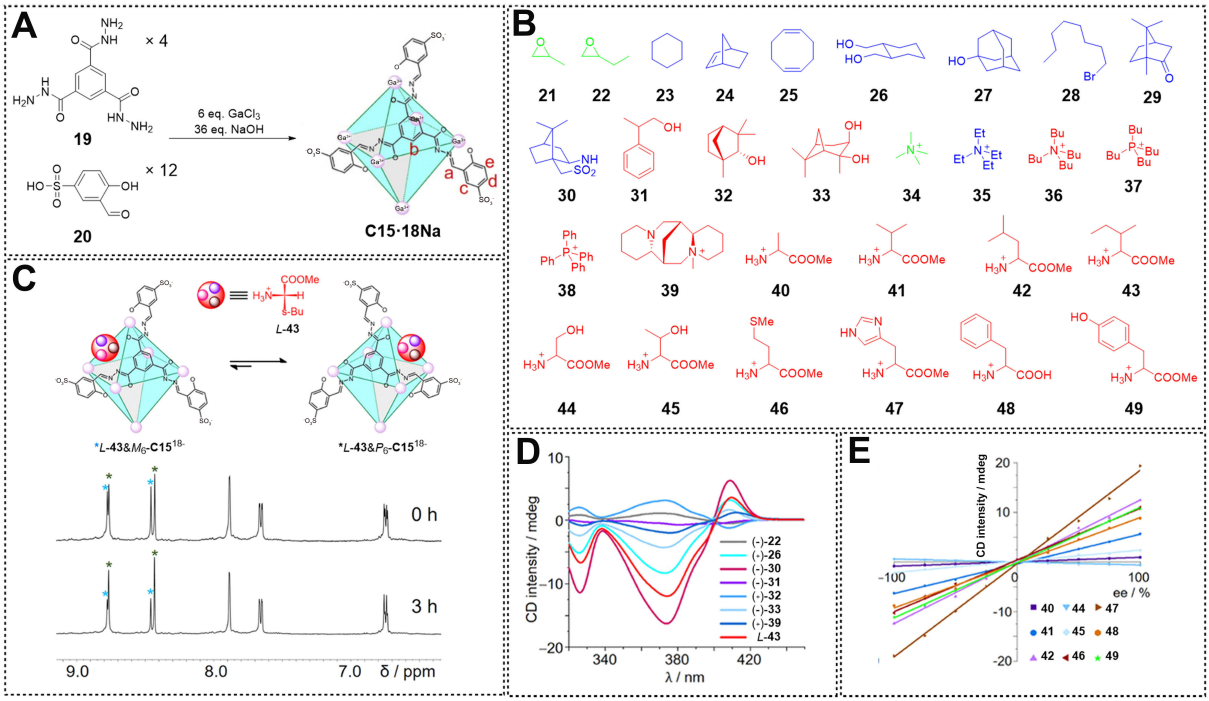

Figure 13. (A) Synthesis of **C15**·18Na; (B) the guests that can be recognized by **C15**$^{18-}$; (C) partial ^{1}H NMR spectra of the mixture of **C15·18Na** and *L*-**43**; (D) calibration curves of the induced CD signal intensities at 380 nm *vs.ee* values for nine a-ammonium ester guests; and (E) CD spectra of **C15·18Na** in presence of chiral guests. NMR: Nuclear magnetic resonance; CD: circular dichroism; *ee*: enantiomeric excess.

superior to the other one after the recognition of chiral guests, both internally and externally, generating CD signals for chiral sensing. The *ee* values of different enantiomeric mixtures could be accurately determined by recording the intensity of the CD signals [Figure 13E].

Chiral cages can be further converted into metal-organic frameworks (MOFs), and in the meantime, their properties can be introduced into these frameworks. Chen *et al.* have done a lot of excellent work in this field[115-117]. In 2017, He *et al.* synthesized self-assembled racemic metal cages derived from Ti^{4+} and ligand **L13** (**L13** = 4,4'-methylenebis(3-hydroxy-2-naphthoic acid)), which could be separated into ***ΔΔΔΔ***-[Ti_4**L13**$_6$] and ***ΛΛΛΛ***-[Ti_4**L13**$_6$] by introducing left-handed [Ag_4(**R-L**)$_5$]$^{4+}$ [R-L = (*1R,2R*)-1,2-diaminocyclohexane] and right-handed [Ag_4(**S-L**)$_5$]$^{4+}$ [S-L = (*1S,2S*) -1,2-diaminocyclohexane] through crystallization[118]. In 2023, Chen *et al.* used $Zn(CH_3COO)_2{\cdot}2H_2O$ and bimb (bimb=4,4'-di(1H-imidazol-1-yl)-1,1'-biphenyl) as tools to connect *ΔΔΔΔ*-[Ti_4L13$_6$] and ***ΛΛΛΛ***-[Ti_4**L13**$_6$], which were reacted for six hours in a mixed solution of H_2O, $NH_3{\cdot}H_2O$, and 1,4-dioxane to obtain **MOF-1**(*Δ*) and **MOF-1**(*Λ*), respectively[119]. Based on the structural analysis, each ***ΛΛΛΛ***-[Ti_4**L13**$_6$] within the framework accommodated three Zn^{II} ions, with uncoordinated carboxylate O atoms situated at the vertices of a tetrahedron. Furthermore, all bimb ligands engaged in coordination in a bidentate mode. The 3D porous architecture of **MOF-1**(*Λ*) primarily relied on the usage of ***ΛΛΛΛ***-[Ti_4**L13**$_6$] in conjunction with three-stranded right-handed helical Zn-bimb chains [Figure 14A]. Noteworthy, the bimb ligand could promote the connection between Zn atoms, forming infinite helical chains along the *C*-axis in **MOF-1**(*Λ*). Interestingly, various guests could form hydrogen bonds with the host and be encapsulated because **MOF-1**(*Λ*) contained a large number of oxygen and nitrogen atoms. Each ***ΛΛΛ Λ***-[Ti_4**L13**$_6$] in **MOF-1**(*Λ*) had two binding sites that could bind to guests due to its twisted structure. Further experiments had shown that the enantiomers of 1-phenethylalcohol (PEOH), 1-phenyl-1-propanol (PPOH), 1-phenyl-1-butanol (PBA), and 1-(4-fluorophenyl)ethanol (FPEOH) could be effectively separated

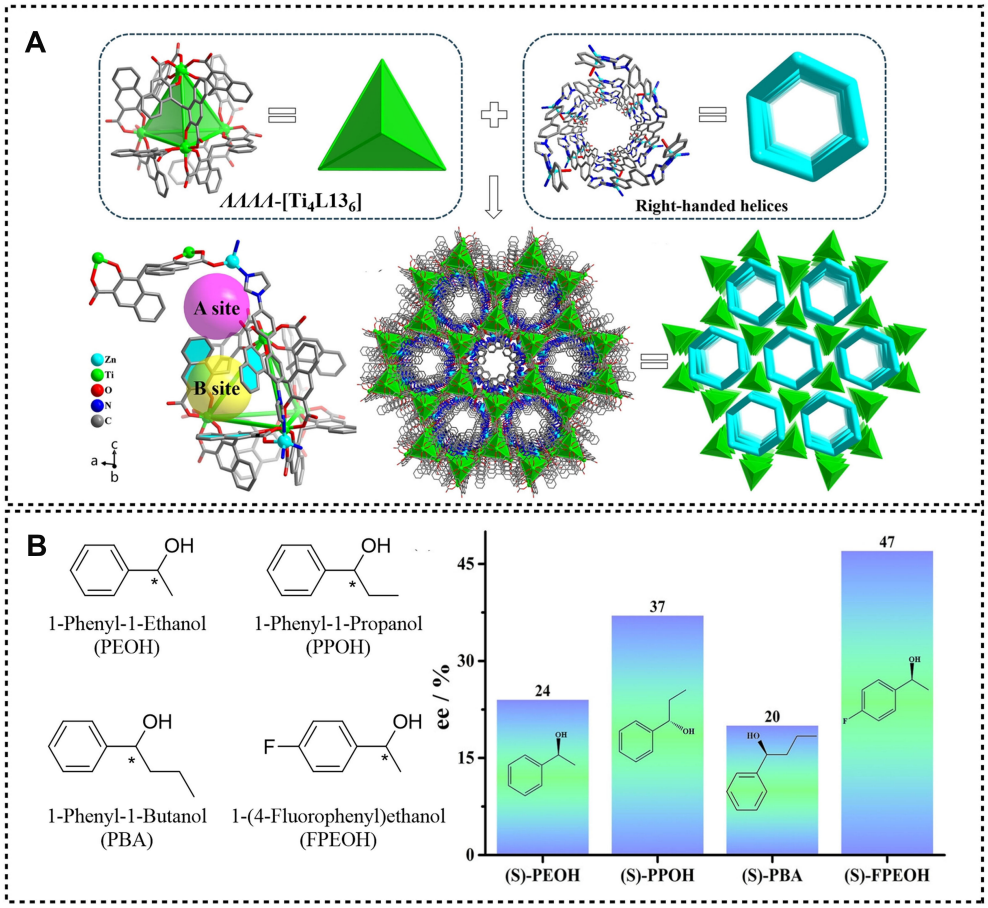

Figure 14. (A) Crystal structures of ΛΛΛΛ-**[Ti_4L13_6]** and the triple-stranded right-handed helical chains along the *C*-axis formed by 4,4′-di(1H-imidazol-1-yl)-1,1′-biphenyl (bimb) ligands and Zn^{II}, coordination environment of the **Ti_4L13_6** cage in **MOF-1**(*Λ*) and 3D framework and simplified structure with helical chiral channels; (B) structures of four guests and results of separation experiments.

by **MOF-1**(*Λ*) respectively, as diverse guest configurations had distinct binding abilities with **MOF-1**(*Λ*) [Figure 14B]. The ability of **MOF-1**(*Λ*) to capture guests was endowed by hydrogen bondings and *π*-*π* interactions. Additionally, various aromatic isomers and nitrile derivatives could be captured by **MOF-1**(*Λ*), such as benzene, toluene, benzonitrile, 3,5-dichlorobenzonitrile, and so on. Interestingly, the isomers of linear *cis*-nitrile and *trans*-nitrile derivatives could also be separated by **MOF-1**(*Λ*). This work provided new ideas and methods for the post modification of chiral metal-organic cages and their application in guest recognition and separation.

CHIRAL GUEST-INDUED CHIROPTICAL RESPONSE WITH PROCHIRAL CAGES

Generating enantiopure chiral host-guest complexes by combining achiral hosts and guests provides a new method for recognizing enantiomers, which is also widely used in MOF, covalent organic frameworks (COF), and small molecule materials[120-122]. However, research on the recognition and separation of enantiomers through prochiral cages is very limited. Unlike the two types of cages mentioned above, the cages introduced in this section are not chiral molecules. It is worth noting that the flexible structures of cages grant them a potential chirality factor. The flipping of units on the cage can induce chirality when introducing chiral guests. Therefore, the changes in CD signals can serve as a basis for determining the configuration of the guests. The advantage of this method is that it reduces the difficulty of synthesizing and separating chiral cages. The disadvantage is also obvious. Although the configuration of the guests can be recognized by the changes in the CD signal, there is still a major challenge for separating the guests.

In 2018, three-layer cyclophanes **C16** and **C17** with a plane of hexakis(phenylethynyl)benzene (HPEB) stacked between two planes of 1,3,5-tris(phenylethynyl)benzene (TPEB) were synthesized by Katoono *et al.* [Figure 15A][123]. The authors used terephthalamide units as bridges because two carbonyl groups of each terephthalamide unit could induce distortion relative to the central benzene core. Specifically, the two amide groups could undergo co-rotational twisting in both directions and provide a dynamic pair of local enantiomeric conformations within the bridge, and three planes were connected by a triple bridge in this molecule. In addition, every two planes could be stacked together and rotate clockwise or counterclockwise, which enabled them to form a pair of enantiomeric conformations with (*M*) - or (*P*) - helicity [Figure 15B]. When the configuration of the molecular cage was *P, P* or *M, M*, it would exist in the form of an enantiomer. However, if its configuration was *P, M*, it would form a *meso*-cage due to the mutual cancellation of these two conformations. More importantly, chiral elements could be introduced into the cage when **(*R,R*)-50** or **(S,*S*)-50** was selected as a chiral group, and the conclusion could be supported by experimental evidence from CD measurements [Figure 15C]. There was a noticeable increase of the CD signal, which could be attributed to the formation of hydrogen bonds between the guest molecule and the host when compound **(*R,R*)-50** or **(*S,S*)-50** was added to the cage, causing the twisting of the bonding arrangement and altering the planar configuration. In addition, the chiral transformation of the cage could also be achieved by changing the temperature [Figure 15D] despite the energy of the racemic cages lower than that of the chiral cages. Only minor Cotton effects were observed at a temperature of 263 K but the Cotton effects steadily grew stronger when the temperature increased to above 273 K due to the formation of *meso*-like substances at lower temperatures. This work provided new methods and ideas for using prochiral cages for enantioselective recognition of chiral guests.

Recently, a cage with a large cavity and multiple binding sites was reported by Hu *et al.*[124]. The synthesized cage was proved to contain three diarylthiourea arms and two 1,3,5-triacylbenzene caps. The addition of CF_3 groups to the cage was implemented to further enhance the acidity and capability of the thiourea groups to bind with anions [Figure 16A]. As shown in Figure 16B, 1,3,5- anion could be encapsulated in the cage due to the formation of multiple hydrogen bonds between the host and guest, and the single crystal structures displayed the conformations of the host-guest complex enantiomers. The 1,3,5-triacylbenzene caps underwent clockwise or counterclockwise rotation, and the thiourea group configuration changed after successfully encapsulating the guest, resulting in the cage to be a pair of enantiomers [Figure 16C]. Subsequently, 1,3,5-benzenetricarboxylate anion derivatives with six chiral centers were synthesized to further test the ability of chiral cages for enantioselective recognition of chiral guests. Interestingly, a strong Cotton effect was observed in the CD spectrum after adding enantiopure **52** and **53** respectively, indicating the effective encapsulation performance of the host molecules [Figure 16D]. Notably, the chiral recognition ability of this prochiral cage was generated by introducing chiral groups in the guest, which guided the cage to rotate in a single direction and ultimately created a chiral environment for guest encapsulation. The main mechanisms of binding, conformational adaptation, and precise stereo control exhibited similarities with a series of biological systems. These similarities could provide valuable insights for designing and constructing functional supramolecular systems.

In 2022, a prochiral supramolecular cage with two tetrastyrene units was designed and constructed by Cheng *et al.*[125]. These two units adopted the *P* and *M* configurations respectively, which resulted in the cage molecule being mesomeric [Figure 17A]. The developed cages possessed potential applications in enantioselective recognition of chiral guests [Figure 17B] due to the flipping of *P* and *M* configurations. Meanwhile, the ability of the cages to encapsulate the guest could be attributed to the hydrophobic effect

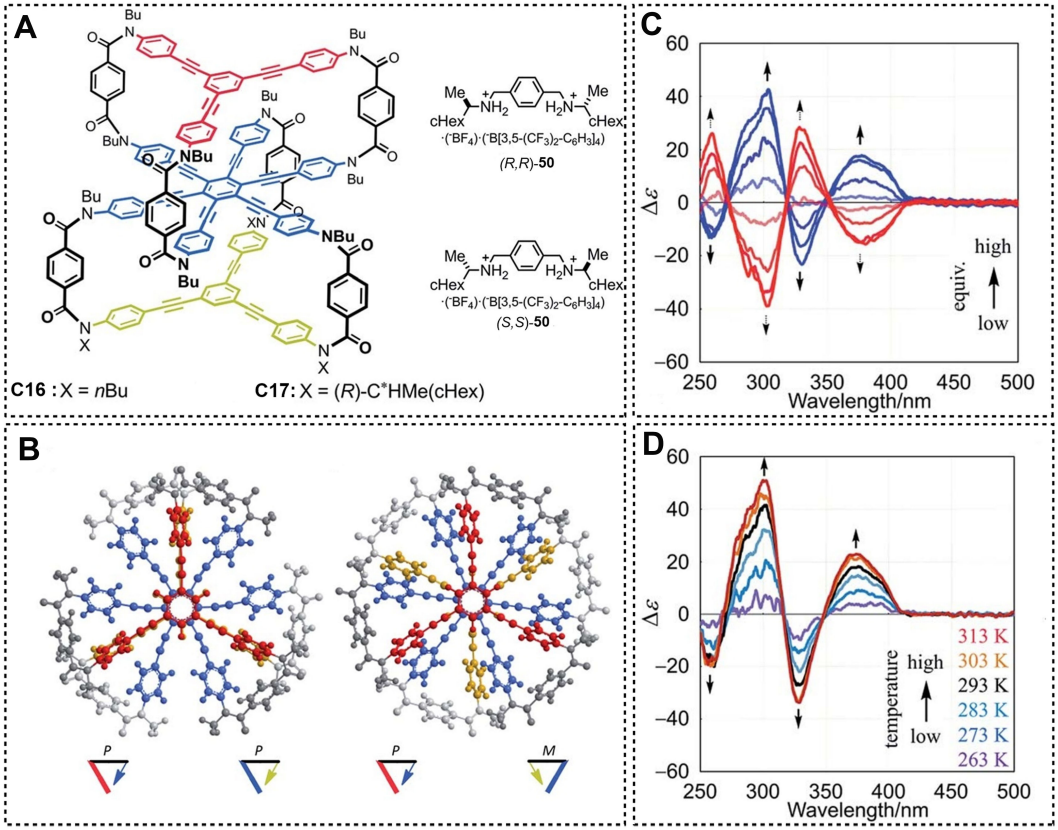

Figure 15. (A) Chemical structures of **C16** and **C17**, and chiral ditopic guests **(*R*,*R*)-50**/**(*S*,*S*)-50**; (B) the most energy-minimized structures for a three-layer model with double-helical form (left) and *meso*-like form (right); (C) CD spectra of **C16** in the presence of a chiral guest **(*S*,*S*)-50** (red lines) or **(*R*,*R*)-50** (blue lines); and (D) VT CD spectra of **C16** in the presence of **(*R*,*R*)-50**. CD: Circular dichroism; VT: variable temperature.

and the mutual attraction with negative ions based on the positive charge on the pyridine group. Further experiments showed that the cage could encapsulate a series of chiral deoxynucleotides in a 1:2 ratio. As the ^{1}H NMR experiments shown in Figure 17C, the significant upfield displacements of the guest molecule were observed clearly due to the shielding effect, indicating the complete encapsulation of the guest. Interestingly, H^a and H^c exhibited different displacement trends based on distinct host/guest ratios, suggesting the two processes of host-guest binding behavior. More importantly, an *M*-shaped tetrastyrene unit on the cage flipped to a *P*-shaped unit in order to better bind with the guest.

As shown in Figure 18, the CD signal of *PP*-**C19**⊃$\mathbf{A}_2$, *PP*-**C19**⊃$\mathbf{T}_2$ and *PP*-**C19**⊃$\mathbf{C}_2$ strengthened gradually with the addition of **A**, **T**, and **C**, which indicated the transformation of the cage from achirality to chirality. Interestingly, compounds 1:1 and 1:2 exhibited opposite CD signals, providing evidence for the two-step binding process of *PP*-**C19**⊃$\mathbf{G}_2$. Meanwhile, *PP*-**C19**⊃$\mathbf{A}_2$, *PP*-**C19**⊃$\mathbf{T}_2$ and *PP*-**C19**⊃$\mathbf{C}_2$ also exhibited excellent CPL signals, strongly correlated with CD signals.

Encouraged by the above work, Cheng *et al.* further explored the wider range of guest molecules[126] [Figure 19A]. The host-guest complexes displayed high binding constants, when the guest molecules were replaced by diverse peptides such as aromatic tryptophan (Trp), phenylalanine (Phe), or tyrosine (Tyr) derivatives [Figure 19B-J]. As shown in Figure 19A, three types of enantiomeric aromatic dipeptides, namely *D*/*L*-TrpTrp, *D*/*L*-PhePhe, and *D*/*L*-TyrTyr, were chosen to explore the chiral adaptability of cage

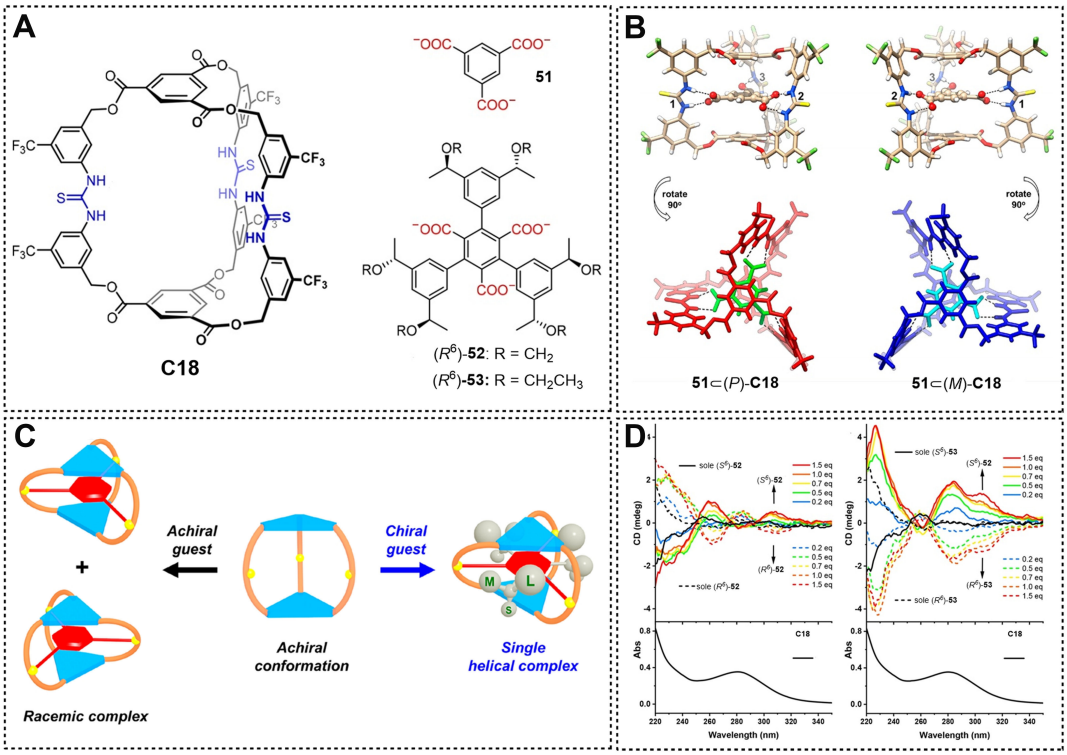

Figure 16. (A) Structure of cage **C18** and anion guests **51-53**; (B) crystal structures of [**51**⊂**C18**]$^{3-}$ showing a racemic mixture of (left) *P*-helical and (right) *M*-helical complexes; (C) schematic representation of guest-induced conformational adaption and gear-like chirality transmission in the adaptive molecular cage; and (D) CD spectra of cage **C18** upon addition of different amounts of chiral guests **52** and **53**. The UV-Vis spectrum of cage **C18** was shown in the bottom. CD: Crcular dichroism; UV-Vis: ultraviolet-visible.

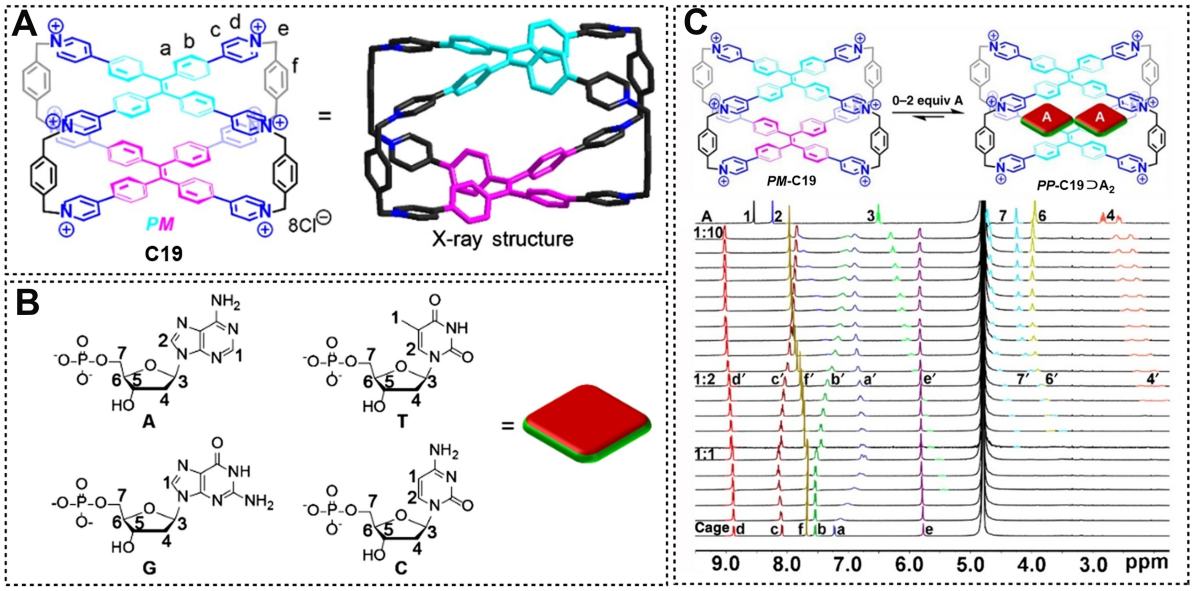

Figure 17. (A) Chemical structures of **C19** and deoxynucleotides (**A**, **T**, **G**, and **C**); (B) schematic representation of the formation of **C19**⊃**A**$_2$; (C) ^{1}H NMR titration of **C19** with **A**.

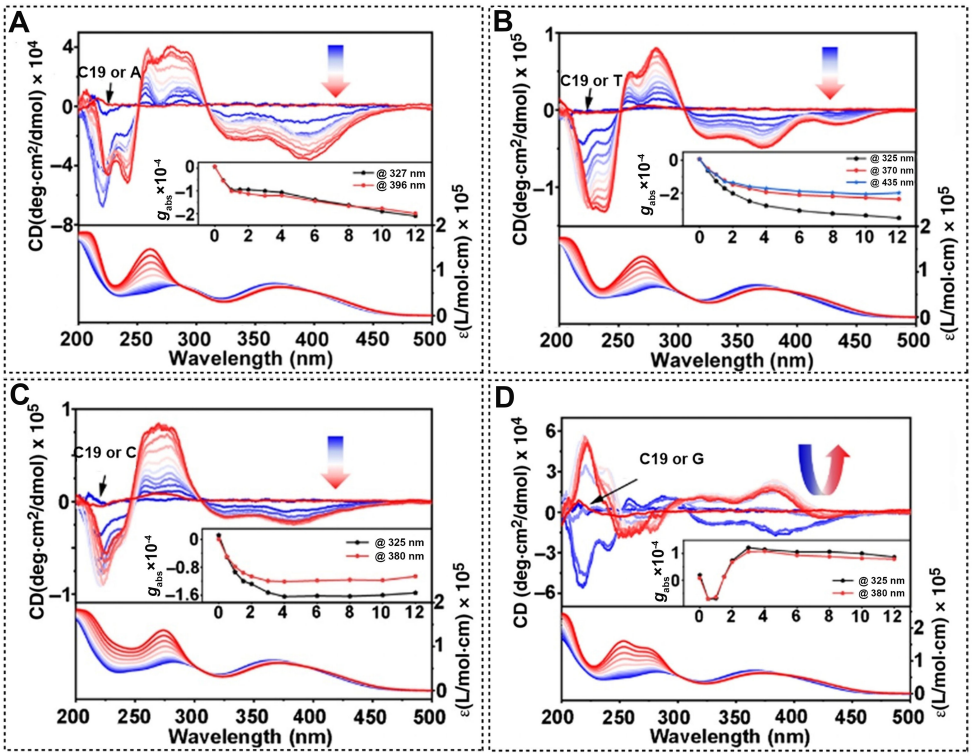

Figure 18. CD titration of **C19** with guests in water: (A) **A**; (B) **T**; (C) **C**; (D) **G**. Inset: Plots of g_{abs} *vs.* the equiv of guests. CD: Crcular dichroism.

C19 through CD titration experiments. The CD spectra of cage **C19** exhibited a prominently positive Cotton effect in the longer wavelength range from 310 nm to 450 nm, which could be attributed to the *M*-rotational conformation of the tetraphenylethylene (TPE) units [Figure 19B and D]. On the other hand, the CD spectra displayed negative signals from 310 to 450 nm, corresponding to the P-rotational conformation of the TPE units when cage **C19** was mixed with *L*-TrpTrp and *L*-PhePhe, respectively. [Figure 19C and E]. These findings also provided compelling evidence that the inherent chirality of *D*/*L*-TrpTrp and *D*/*L*-PhePhe played a crucial role in determining the specific rotational conformation transformation and led to *MM*-**C19** and *PP*-**C19**, respectively. The obvious changes in the CD spectrum [Figure 19F] were also observed when the guest molecules were replaced with PhePhePhe and TyrTyrTyr, respectively. The authors also achieved a calibration curve with high linearity ($R^2 > 0.99$) by plotting the CD signals of three pairs of enantiomers at 390 nm against the *ee* values. The errors associated with these measurements ranged from 1.22% to 3.68% [Figure 19G], and the calibration lines could be utilized to accurately determine the enantiopurity of dipeptide enantiomers. Furthermore, a noticeable decrease of fluorescence intensity at 560 nm was observed for **C19** due to photoinduced electron transfer (PET) between the electron-deficient pyridinium rings and the electron-rich indole rings of *L*-TrpTrp [Figure 19H]. On the other hand, introducing *L*-PhePhe into the phosphate buffer solution of **C19** increased fluorescence intensity at 560 nm, which could be attributed to the restriction of intramolecular rotation (RIR) mechanism when PhePhe molecules were inserted into the inner cavity of **C19** [Figure 19I], and the host-guest complexes of PhePhePhe and TyrTyrTyr with **C19** both exhibited CPL signals [Figure 19J].

SUMMARY AND OUTLOOK

We summarized the diverse synthesis of chiral cage materials with tailored functionalities and their

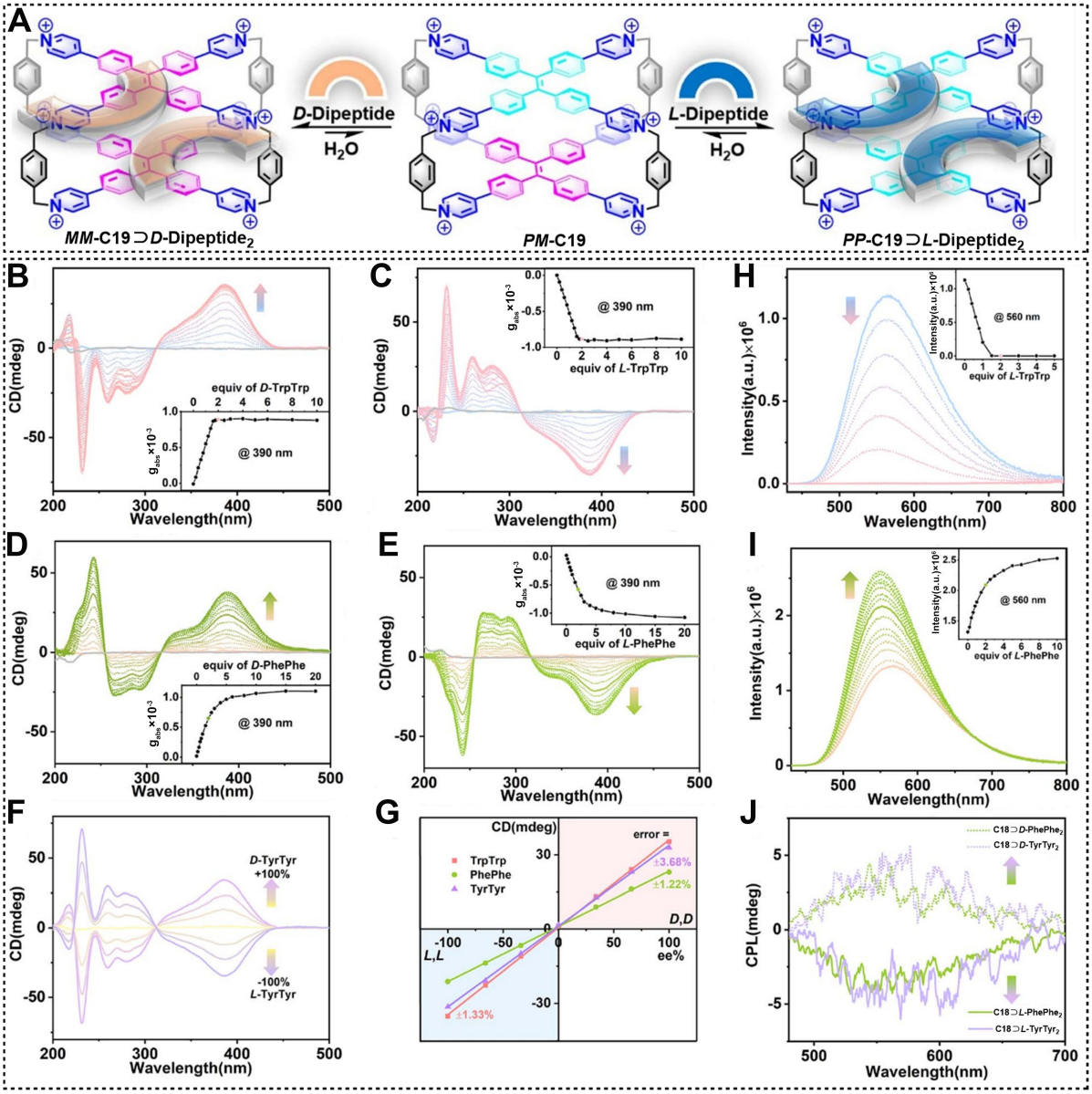

Figure 19. (A) Schematic representation of the chiral adaptive recognition of **C19** for *D*/*L*-dipeptides; CD spectra of **C19** titrated with (B) *D*-TrpTrp, (C) *L*-TrpTrp, (D) *D*-PhePhe, and (E) *L*-PhePhe in phosphate buffer. (Inset) Plots of gabs *vs.* equiv. of guests; (F) CD spectra of **C19** in the presence of *D*/*L*-TyrTyr mixtures with *ee* ranging from -100% to +100%. (G) The calibration curve obtained for the CD signals (390 nm) upon varying *ee* values for *D*/*L*-dipeptides; Fluorescence spectra of **C19** titrated with (H) *L*-TrpTrp and (I) *L*-PhePhe in phosphate buffer. (Inset) Plots of fluorescence intensity *vs.* equiv. of guests; (J) CPL spectra of **C19** with *D*/*L*-PhePhe (chartreuse) and *D*/*L*-TyrTyr (light purple) in phosphate buffer. CD: Crcular dichroism; *ee*: enantiomeric excess; CPL: circularly polarized luminescence.

applications in enantioselective recognition and separation. The research related to enantioselective separation based on chiral cages has made great progress since their discovery, and they have also been widely used in chemistry, pharmacy, agriculture, environmental science, materials science, and clinical medicine. The special structures of chiral cages play important roles in recognizing and separating enantiomers. So far, their synthesis using diverse methods has been extensively reported. However, much work remains to be done about the assembly strategy and chiral behavior of chiral cages. How to obtain chiral retention, enhancement, transfer and amplification of preconditioned chiral units through the subtle design and layout of the metal nodes and ligand linkages? How to control the preparation and

crystallization conditions to obtain homochiral cages and put them into practice? In addition, we should focus on developing environmentally friendly strategies to improve the chiral recognition and separation performance in future research. Exploring new structures and materials, adjusting energy levels and electron transfer behavior, and controlling structure and aggregation will be effective strategies for further applications. Therefore, addressing these issues is fascinating and challenging. From the view of green chemistry, it is desirable to develop sustainable strategies for synthesis of chiral cage materials with tailored functionalities and explore their applications. Last but not least, the enantioselective recognition and separation based on chiral cage materials remains a hot topic and frontier in chemistry. We hope this review could facilitate further breakthroughs from the wider community of synthetic material chemistry in this exciting field.

DECLARATIONS

Acknowledgments

We acknowledge the Molecular Scale Lab for mass spectrometry characterization.

Authors' contributions

Writing the manuscript and being responsible for the whole work: Shi L, Guo Y
Revising the first draft of the manuscript: Li T, Ding L, Kang Y, Hao XQ, Pan Y

Availability of data and materials

Not applicable.

Financial support and sponsorship

This research was funded by the National Natural Science Foundation of China (No. 22101267), the Natural Science Foundation of Henan Province (No. 202300410477), and the China Postdoctoral Science Foundation (No. 2021M692905).

Conflicts of interest

All authors declared that there are no conflicts of interest.

Ethical approval and consent to participate

Not applicable.

Consent for publication

Not applicable.

REFERENCES

1. Li Y, Wang X, Miao J, et al. Chiral Transition Metal Oxides: Synthesis, Chiral Origins, and Perspectives. *Adv Mater* 2020;32:e1905585. DOI
2. Simeonov SP, Nunes JP, Guerra K, Kurteva VB, Afonso CA. Synthesis of chiral cyclopentenones. *Chem Rev* 2016;116:5744-893. DOI PubMed
3. Xue YP, Cao CH, Zheng YG. Enzymatic asymmetric synthesis of chiral amino acids. *Chem Soc Rev* 2018;47:1516-61. DOI PubMed
4. H RT. Salvarsan or 606 (dioxy-diamino-arsenobenzol): its chemistry, pharmacy, and therapeutics. *Nature* 1911;86:412. DOI
5. Oliveira AL, Viegas MF, da Silva SL, Soares AM, Ramos MJ, Fernandes PA. The chemistry of snake venom and its medicinal potential. *Nat Rev Chem* 2022;6:451-69. DOI PubMed
6. Wang X. Indole alkaloid synthesis via radical cascade reactions. *Chem* 2017;2:749-50. DOI

7. Rice CP, McCarty GW, Bialek-Kalinski K, Zabetakis K, Torrents A, Hapeman CJ. Corrigendum to "Analysis of metolachlor ethane sulfonic acid (MESA) chirality in groundwater: a tool for dating groundwater movement in agricultural settings" [Sci. Total Environ. 560-561 (2016) 36-43]. *Sci Total Environ* 2016;742:140736. DOI PubMed
8. Zhang H, Spiteller M, Guenther K, Boehmler G, Zuehlke S. Degradation of a chiral nonylphenol isomer in two agricultural soils. *Environ Pollut* 2009;157:1904-10. DOI PubMed
9. Zhang Q, Zhang Z, Tang B, et al. Mechanistic insights into stereospecific bioactivity and dissipation of chiral fungicide triticonazole in agricultural management. *J Agric Food Chem* 2018;66:7286-93. DOI
10. Barreiro JC, Tiritan ME, Cass QB. Challenges and innovations in chiral drugs in an environmental and bioanalysis perspective. *TrAC Trends Anal Chem* 2021;142:116326. DOI
11. Fu Y, Borrull F, Marcé RM, Fontanals N. Enantiomeric fraction determination of chiral drugs in environmental samples using chiral liquid chromatography and mass spectrometry. *Trends Environ Anal Chem* 2021;29:e00115. DOI
12. Sanganyado E, Lu Z, Fu Q, Schlenk D, Gan J. Chiral pharmaceuticals: a review on their environmental occurrence and fate processes. *Water Res* 2017;124:527-42. DOI
13. Duan Y, Che S. Chiral mesostructured inorganic materials with optical chiral response. *Adv Mater* 2023;35:e2205088. DOI PubMed
14. Gu ZG, Zhan C, Zhang J, Bu X. Chiral chemistry of metal-camphorate frameworks. *Chem Soc Rev* 2016;45:3122-44. DOI PubMed
15. Kuang H, Xu C, Tang Z. Emerging chiral materials. *Adv Mater* 2020;32:e2005110. DOI PubMed
16. Bentley R. Role of sulfur chirality in the chemical processes of biology. *Chem Soc Rev* 2005;34:609-24. DOI PubMed
17. Hussain M, Rupp F, Wendel HP, Gehring FK. Bioapplications of acoustic crystals, a review. *TrAC Trends Anal Chem* 2018;102:194-209. DOI
18. Nau C, Strichartz GR. Drug chirality in anesthesia. *Anesthesiology* 2002;97:497-502. DOI PubMed
19. Caban M, Stepnowski P. How to decrease pharmaceuticals in the environment? A review. *Environ Chem Lett* 2021;19:3115-38. DOI
20. Kar S, Sanderson H, Roy K, Benfenati E, Leszczynski J. Green chemistry in the synthesis of pharmaceuticals. *Chem Rev* 2022;122:3637-710. DOI PubMed
21. Kelly SA, Pohle S, Wharry S, et al. Application of ω-transaminases in the pharmaceutical industry. *Chem Rev* 2018;118:349-67. DOI
22. Pilz M, Cavelius P, Qoura F, Awad D, Brück T. Lipopeptides development in cosmetics and pharmaceutical applications: a comprehensive review. *Biotechnol Adv* 2023;67:108210. DOI PubMed
23. Wang G, Ang HT, Dubbaka SR, O'Neill P, Wu J. Multistep automated synthesis of pharmaceuticals. *Trends Chem* 2023;5:432-45. DOI
24. Hu M, Feng H, Yuan Y, Zheng Y, Tang BZ. Chiral AIEgens - Chiral recognition, CPL materials and other chiral applications. *Coord Chem Rev* 2020;416:213329. DOI
25. Pop F, Zigon N, Avarvari N. Main-group-based electro- and photoactive chiral materials. *Chem Rev* 2019;119:8435-78. DOI PubMed
26. Xue M, Li B, Qiu S, Chen B. Emerging functional chiral microporous materials: synthetic strategies and enantioselective separations. *Mater Today* 2016;19:503-15. DOI
27. Zhang Q, Xue S, Li A, Ren S. Functional materials in chiral capillary electrophoresis. *Coord Chem Rev* 2021;445:214108. DOI
28. Zhang Y, Yu S, Han B, et al. Circularly polarized luminescence in chiral materials. *Matter* 2022;5:837-75. DOI
29. Tay HM, Kyratzis N, Thoonen S, Boer SA, Turner DR, Hua C. Synthetic strategies towards chiral coordination polymers. *Coord Chem Rev* 2021;435:213763. DOI
30. Zhang G, Cheng X, Wang Y, Zhang W. Supramolecular chiral polymeric aggregates: construction and applications. *Aggregate* 2023;4:e262. DOI
31. Chen LJ, Yang HB, Shionoya M. Chiral metallosupramolecular architectures. *Chem Soc Rev* 2017;46:2555-76. DOI PubMed
32. Feng HT, Yuan YX, Xiong JB, Zheng YS, Tang BZ. Macrocycles and cages based on tetraphenylethylene with aggregation-induced emission effect. *Chem Soc Rev* 2018;47:7452-76. DOI PubMed
33. Jędrzejewska H, Szumna A. Making a right or left choice: chiral self-sorting as a tool for the formation of discrete complex structures. *Chem Rev* 2017;117:4863-99. DOI PubMed
34. Pan M, Wu K, Zhang J, Su C. Chiral metal-organic cages/containers (MOCs): from structural and stereochemical design to applications. *Coord Chem Rev* 2019;378:333-49. DOI
35. Van Der Voort P, Esquivel D, De Canck E, Goethals F, Van Driessche I, Romero-Salguero FJ. Periodic Mesoporous Organosilicas: from simple to complex bridges; a comprehensive overview of functions, morphologies and applications. *Chem Soc Rev* 2013;42:3913-55. DOI PubMed
36. Zhang D, Ronson TK, Zou YQ, Nitschke JR. Metal-organic cages for molecular separations. *Nat Rev Chem* 2021;5:168-82. DOI PubMed
37. Borsley S, Haugland MM, Oldknow S, et al. Electrostatic forces in field-perturbed equilibria: nanopore analysis of cage complexes. *Chem* 2019;5:1275-92. DOI
38. Cooper JA, Borsley S, Lusby PJ, Cockroft SL. Discrimination of supramolecular chirality using a protein nanopore. *Chem Sci* 2017;8:5005-9. DOI PubMed PMC
39. Kovalska VB, Vakarov SV, Kuperman MV, et al. Induced chirality of cage metal complexes switched by their supramolecular and covalent binding. *Dalton Trans* 2018;47:1036-52. DOI
40. Li B, Zheng B, Zhang W, Zhang D, Yang XJ, Wu B. Site-selective binding of peripheral chiral guests induces stereospecificity in

A_4L_6 tetrahedral anion cages. *J Am Chem Soc* 2020;142:6304-11. DOI PubMed

41. Li Y, Dong J, Gong W, et al. Artificial biomolecular channels: enantioselective transmembrane transport of amino acids mediated by homochiral zirconium metal-organic cages. *J Am Chem Soc* 2021;143:20939-51. DOI PubMed
42. Jiao J, Tan C, Li Z, Liu Y, Han X, Cui Y. Design and assembly of chiral coordination cages for asymmetric sequential reactions. *J Am Chem Soc* 2018;140:2251-9. DOI
43. Luo N, Ao YF, Wang DX, Wang QQ. Exploiting anion-π interactions for efficient and selective catalysis with chiral molecular cages. *Angew Chem Int Ed Engl* 2021;60:20650-5. DOI PubMed
44. Tan C, Chu D, Tang X, Liu Y, Xuan W, Cui Y. Supramolecular coordination cages for asymmetric catalysis. *Chemistry* 2019;25:662-72. DOI
45. Tan C, Jiao J, Li Z, Liu Y, Han X, Cui Y. Design and assembly of a chiral metallosalen-based octahedral coordination cage for supramolecular asymmetric catalysis. *Angew Chem Int Ed Engl* 2018;57:2085-90. DOI PubMed
46. Wang Y, Sun Y, Shi P, et al. Chaperone-like chiral cages for catalyzing enantio-selective supramolecular polymerization. *Chem Sci* 2019;10:8076-82. DOI PubMed PMC
47. Zhang D, Martinez A, Dutasta JP. Emergence of hemicryptophanes: from synthesis to applications for recognition, molecular machines, and supramolecular catalysis. *Chem Rev* 2017;117:4900-42. DOI PubMed
48. Deng DR, Li C, Weng JC, et al. Thin nano cages with limited hollow space for ultrahigh sulfur loading lithium-sulfur batteries. *ACS Appl Mater Interfaces* 2022;14:45414-22. DOI PubMed
49. Li H, Huang Y, Zhang Y, et al. An ultrathin functional layer based on porous organic cages for selective ion sieving and lithium-sulfur batteries. *Nano Lett* 2022;22:2030-7. DOI PubMed
50. Li J, Qi J, Jin F, et al. Room temperature all-solid-state lithium batteries based on a soluble organic cage ionic conductor. *Nat Commun* 2022;13:2031. DOI PubMed PMC
51. Li X, Xu D, Wang A, Peng C, Liu X, Luo J. Metal-organic cage as fluorescent probe for $LiPF_6$ in lithium batteries. *Green Energy Environ* 2023;In Press. DOI
52. Peng L, Sun Y, Guo S, Li C. Correction: highly efficient construction of hollow Co-N*x* nanocube cage dispersion implanted with porous carbonized nanofibers for Li-O_2 batteries. *J Mater Chem A* 2022;10:740-51. DOI
53. Zhang L, Jia Y, Meng F, et al. A naphthalene organic cage captured sodium polysulphide as cathode materials for lithium-ion sulfide batteries. *J Alloys Compd* 2022;923:166488. DOI
54. Zhang X, Su K, Mohamed AGA, et al. Photo-assisted charge/discharge Li-organic battery with a charge-separated and redox-active C_{60}@porous organic cage cathode. *Energy Environ Sci* 2022;15:780-5. DOI
55. Li W, Zhou Y, Gao T, et al. Circularly polarized luminescent $Eu_4(L^R)_4$ cage for enantiomeric excess and concentration simultaneous determination of chiral diamines. *ACS Appl Mater Interfaces* 2022;14:55979-88. DOI PubMed
56. Sun YL, Wang Z, Ma H, et al. Chiral emissive porous organic cages. *Chem Commun* 2023;59:302-5. DOI
57. Tang X, Jiang H, Si Y, et al. Endohedral functionalization of chiral metal-organic cages for encapsulating achiral dyes to induce circularly polarized luminescence. *Chem* 2021;7:2771-86. DOI
58. Wu K, Tessarolo J, Baksi A, Clever GH. Guest-modulated circularly polarized luminescence by ligand-to-ligand chirality transfer in heteroleptic Pd^{II} coordination cages. *Angew Chem Int Ed Engl* 2022;61:e202205725. DOI PubMed PMC
59. Zheng A, Zhao T, Jin X, Miao W, Duan P. Circularly polarized luminescent porous crystalline nanomaterials. *Nanoscale* 2022;14:1123-35. DOI PubMed
60. Chen SQ, Zhai QG, Li SN, Jiang YC, Hu MC. Channel partition into nanoscale polyhedral cages of a triple-self-interpenetrated metal-organic framework with high CO2 uptake. *Inorg Chem* 2015;54:10-2. DOI PubMed
61. Goronzy DP, Staněk J, Avery E, et al. Influence of terminal carboxyl groups on the structure and reactivity of functionalized *m*-carboranethiolate self-assembled monolayers. *Chem Mater* 2020;32:6800-9. DOI
62. Grunder S, Valente C, Whalley AC, et al. Molecular gauge blocks for building on the nanoscale. *Chemistry* 2012;18:15632-49. DOI
63. Stang PJ, Olenyuk B, Muddiman DC, Smith RD. Transition-metal-mediated rational design and self-assembly of chiral, nanoscale supramolecular polyhedra with unique *T* symmetry. *Organometallics* 1997;16:3094-6. DOI
64. Chaudhari AK, Tan JC. Mechanochromic MOF nanoplates: spatial molecular isolation of light-emitting guests in a sodalite framework structure. *Nanoscale* 2018;10:3953-60. DOI
65. Bajpayee N, Vijayakanth T, Rencus-Lazar S, et al. Exploring helical peptides and foldamers for the design of metal helix frameworks: current trends and future perspectives. *Angew Chem Int Ed Engl* 2023;62:e202214583. DOI
66. Han D, Yao Z. Chiral mass spectrometry: an overview. *TrAC Trends Anal Chem* 2020;123:115763. DOI
67. Lipkowitz KB. Atomistic modeling of enantioselective binding. *Acc Chem Res* 2000;33:555-62. DOI PubMed
68. Scriba GKE. Chiral recognition in separation sciences. Part II: Macrocyclic glycopeptide, donor-acceptor, ion-exchange, ligand-exchange and micellar selectors. *TrAC Trends Anal Chem* 2019;119:115628. DOI
69. Wang S, Li L, Xiao Y, Wang Y. Recent advances in cyclodextrins-based chiral-recognizing platforms. *TrAC Trends Anal Chem* 2019;121:115691. DOI
70. Zehnacker A, Suhm MA. Chirality recognition between neutral molecules in the gas phase. *Angew Chem Int Ed Engl* 2008;47:6970-92. DOI PubMed
71. Zor E, Bingol H, Ersoz M. Chiral sensors. *TrAC Trends Anal Chem* 2019;121:115662. DOI
72. Zou J, Zhao G, Zhao G, Yu J. Fast and sensitive recognition of enantiomers by electrochemical chiral analysis: recent advances and

future perspectives. *Coord Chem Rev* 2022;471:214732. DOI
73. Berijani K, Chang L, Gu Z. Chiral templated synthesis of homochiral metal-organic frameworks. *Coord Chem Rev* 2023;474:214852. DOI
74. Daintree LS, Kordikowski A, York P. Separation processes for organic molecules using SCF Technologies. *Adv Drug Deliv Rev* 2008;60:351-72. DOI PubMed
75. Fan W, Matsuno T, Han Y, et al. Synthesis and chiral resolution of twisted carbon nanobelts. *J Am Chem Soc* 2021;143:15924-9. DOI
76. Noorduin WL, van der Asdonk P, Meekes H, et al. Complete chiral resolution using additive-induced crystal size bifurcation during grinding. *Angew Chem Int Ed Engl* 2009;48:3278-80. DOI PubMed
77. Xie R, Chu LY, Deng JG. Membranes and membrane processes for chiral resolution. *Chem Soc Rev* 2008;37:1243-63. DOI PubMed
78. Zhou F, Shemchuk O, Charpentier MD, et al. Simultaneous chiral resolution of two racemic compounds by preferential cocrystallization*. *Angew Chem Int Ed Engl* 2021;60:20264-8. DOI PubMed
79. Beaulieu S, Comby A, Descamps D, et al. Photoexcitation circular dichroism in chiral molecules. *Nature Phys* 2018;14:484-9. DOI
80. Kong XT, Khosravi Khorashad L, Wang Z, Govorov AO. Photothermal circular dichroism induced by plasmon resonances in chiral metamaterial absorbers and bolometers. *Nano Lett* 2018;18:2001-8. DOI PubMed
81. Quan M, Pang XY, Jiang W. Circular dichroism based chirality sensing with supramolecular host-guest chemistry. *Angew Chem Int Ed Engl* 2022;61:e202201258. DOI PubMed
82. Zhang Y, Rouxel JR, Autschbach J, Govind N, Mukamel S. X-ray circular dichroism signals: a unique probe of local molecular chirality. *Chem Sci* 2017;8:5969-78. DOI PubMed PMC
83. Guo JX, Yang C, Yan XP. "Thiol-ene" click synthesis of chiral covalent organic frameworks for gas chromatography. *J Mater Chem A* 2021;9:21151-7. DOI
84. Welch CJ. Are we approaching a speed limit for the chromatographic separation of enantiomers? *ACS Cent Sci* 2017;3:823-9. DOI PubMed PMC
85. Yuan C, Jia W, Yu Z, et al. Are highly stable covalent organic frameworks the key to universal chiral stationary phases for liquid and gas chromatographic separations? *J Am Chem Soc* 2022;144:891-900. DOI PubMed
86. Zhou X, Liu Q, Wang H. Chiral resolution of DL-glutamic acid by a chiral additive. *J Chem Tech Biotech* 2022;97:1240-6. DOI
87. Cheng Q, Ma Q, Pei H, Mo Z. Chiral membranes for enantiomer separation: a comprehensive review. *Sep Purif Technol* 2022;292:121034. DOI
88. Wu Q, Lv H, Zhao L. Applications of carbon nanomaterials in chiral separation. *TrAC Trends Anal Chem* 2020;129:115941. DOI
89. Zhang QP, Wang Z, Zhang ZW, et al. Triptycene-based chiral porous polyimides for enantioselective membrane separation. *Angew Chem Int Ed Engl* 2021;60:12781-5. DOI PubMed
90. O'Neil LG, Bower JF. Electrophilic aminating agents in total synthesis. *Angew Chem Int Ed Engl* 2021;60:25640-66. DOI PubMed PMC
91. Wu Q, Sun Y, Gao J, et al. Applications of hybrid organic-inorganic materials in chiral separation. *TrAC Trends Anal Chem* 2017;95:140-8. DOI
92. Yasui M, Ota R, Tsukano C, Takemoto Y. Total synthesis of avenaol. *Nat Commun* 2017;8:674. DOI PubMed PMC
93. Duan C, Cheng Z, Wang B, et al. Chiral photonic liquid crystal films derived from cellulose nanocrystals. *Small* 2021;17:e2007306. DOI
94. Nayani K, Kim YK, Abbott NL. Colloids: chiral interactions in liquid crystals. *Nat Mater* 2017;17:14-5. DOI PubMed
95. Yuan Y, Martinez A, Senyuk B, Tasinkevych M, Smalyukh II. Chiral liquid crystal colloids. *Nat Mater* 2018;17:71-9. DOI PubMed
96. Hou Y, Liang J, Kuang X, Kuang R. Simultaneous electrochemical recognition of tryptophan and penicillamine enantiomers based on MOF-modified β-CD. *Carbohydr Polym* 2022;290:119474. DOI PubMed
97. Zhang L, Wang G, Xiong C, et al. Chirality detection of amino acid enantiomers by organic electrochemical transistor. *Biosens Bioelectron* 2018;105:121-8. DOI
98. Brunel JM. BINOL: a versatile chiral reagent. *Chem Rev* 2005;105:857-97. DOI PubMed
99. Parmar D, Sugiono E, Raja S, Rueping M. Complete field guide to asymmetric BINOL-phosphate derived Brønsted acid and metal catalysis: history and classification by mode of activation; Brønsted acidity, hydrogen bonding, ion pairing, and metal phosphates. *Chem Rev* 2014;114:9047-153. DOI PubMed
100. Ramakrishna E, Tang JD, Tao JJ, et al. Self-assembly of chiral BINOL cages *via* imine condensation. *Chem Commun* 2021;57:9088-91. DOI PubMed
101. Liu C, Jin Y, Qi D, et al. Enantioselective assembly and recognition of heterochiral porous organic cages deduced from binary chiral components. *Chem Sci* 2022;13:7014-20. DOI PubMed PMC
102. Cui DX, Geng Y, Kou JN, et al. Chiral self-sorting and guest recognition of porous aromatic cages. *Nat Commun* 2022;13:4011. DOI PubMed PMC
103. Gingras M. One hundred years of helicene chemistry. Part 1: non-stereoselective syntheses of carbohelicenes. *Chem Soc Rev* 2013;42:968-1006. DOI PubMed
104. Shen Y, Chen CF. Helicenes: synthesis and applications. *Chem Rev* 2012;112:1463-535. DOI
105. Malik AU, Gan F, Shen C, et al. Chiral organic cages with a triple-stranded helical structure derived from helicene. *J Am Chem Soc* 2018;140:2769-72. DOI

106. Schulte TR, Holstein JJ, Clever GH. Chiral self-discrimination and guest recognition in helicene-based coordination cages. *Angew Chem Int Ed Engl* 2019;58:5562-6. DOI PubMed PMC
107. Lei Y, Chen Q, Liu P, et al. Molecular cages self-assembled by imine condensation in water. *Angew Chem Int Ed Engl* 2021;60:4705-11. DOI PubMed
108. Li G, Ronson TK, Lavendomme R, et al. Enantiopure $Fe^{II}_4L_4$ cages bind steroids stereoselectively. *Chem* 2023;9:1549-61. DOI
109. Hou YJ, Wu K, Wei ZW, et al. Design and enantioresolution of homochiral Fe(II)-Pd(II) coordination cages from stereolabile metalloligands: stereochemical stability and enantioselective separation. *J Am Chem Soc* 2018;140:18183-91. DOI PubMed
110. Zhu C, Tang H, Yang K, et al. Homochiral dodecanuclear lanthanide "cage in cage" for enantioselective separation. *J Am Chem Soc* 2021;143:12560-6. DOI PubMed
111. Zhang D, Ronson TK, Greenfield JL, et al. Enantiopure $[Cs^+/Xe\subset cryptophane]\subset Fe^{II}_4L_4$ hierarchical superstructures. *J Am Chem Soc* 2019;141:8339-45. DOI PubMed
112. Xue W, Pesce L, Bellamkonda A, et al. Subtle stereochemical effects influence binding and purification abilities of an $Fe^{II}_4L_4$ cage. *J Am Chem Soc* 2023;145:5570-7. DOI PubMed PMC
113. Hu SJ, Guo XQ, Zhou LP, et al. Guest-driven self-assembly and chiral induction of photofunctional lanthanide tetrahedral cages. *J Am Chem Soc* 2022;144:4244-53. DOI PubMed
114. Wu G, Chen Y, Fang S, et al. A self-assembled cage for wide-scope chiral recognition in water. *Angew Chem Int Ed Engl* 2021;60:16594-9. DOI PubMed
115. Chen H, Gu ZG, Zhang J. Surface chiroselective assembly of enantiopure crystalline porous films containing bichiral building blocks. *Chem Sci* 2021;12:12346-52. DOI PubMed PMC
116. Chen R, Chen G, He Y, Zhang J. Coordination assembly of tetrahedral $Ti_4(embonate)_6$ cages with alkaline-earth metal ions. *Chin J Struct Chem* 2022;41:2201001-6. DOI
117. Teng Q, Xiang G, Chen GH, Chen SM, He YP, Zhang J. Coordination assembly of tetrahedral $Zr_4(embonate)_6$ cages with Eu^{3+} ions. *Inorg Chem* 2021;60:18178-84. DOI PubMed
118. He YP, Yuan LB, Chen GH, et al. Water-soluble and ultrastable Ti_4L_6 tetrahedron with coordination assembly function. *J Am Chem Soc* 2017;139:16845-51. DOI PubMed
119. Chen GH, He YP, Yu Y, et al. Post-assembly modification of homochiral titanium-organic cages for recognition and separation of molecular isomers. *Angew Chem Int Ed Engl* 2023;62:e202300726. DOI PubMed
120. Buhse T, Cruz JM, Noble-Terán ME, et al. Spontaneous deracemizations. *Chem Rev* 2021;121:2147-229. DOI
121. Hou X, Xu T, Wang Y, Liu S, Tong J, Liu B. Superficial chiral etching on achiral metal-organic framework for enantioselective sorption. *ACS Appl Mater Interfaces* 2017;9:32264-9. DOI PubMed
122. Soloshonok VA, Roussel C, Kitagawa O, Sorochinsky AE. Self-disproportionation of enantiomers via achiral chromatography: a warning and an extra dimension in optical purifications. *Chem Soc Rev* 2012;41:4180-8. DOI
123. Katoono R, Obara Y, Fujiwara K, Suzuki T. Enhanced circular dichroism at elevated temperatures through complexation-induced transformation of a three-layer cyclophane with dualistic dynamic helicity. *Chem Sci* 2018;9:2222-9. DOI PubMed PMC
124. Hu QP, Zhou H, Huang TY, Ao YF, Wang DX, Wang QQ. Chirality gearing in an achiral cage through adaptive binding. *J Am Chem Soc* 2022;144:6180-4. DOI
125. Cheng L, Liu K, Duan Y, et al. Adaptive chirality of an achiral cage: chirality transfer, induction, and circularly polarized luminescence through aqueous host-guest complexation. *CCS Chem* 2021;3:2749-63. DOI
126. Cheng L, Tian P, Duan H, et al. Chiral adaptive recognition with sequence specificity of aromatic dipeptides in aqueous solution by an achiral cage. *Chem Sci* 2023;14:833-42. DOI PubMed PMC